8-2010

Characterization of Optically Stimulated Luminescent Detectors in Photon & Proton Beams for Use in Anthropomorphic Phantoms

James R. Kerns

Characterization of Optically Stimulated Luminescent Detectors in Photon & Proton Beams for Use in Anthropomorphic Phantoms

By

James R. Kerns, B.S.

APPROVED:

_____
Geoffrey S. Ibbott, Ph.D.
Supervisory Professor

_____
David S. Followill, Ph.D.

_____
Narayan Sahoo, Ph.D.

_____
Stephen Kry, Ph.D.

_____
Valen Johnson, Ph.D.

APPROVED:

_____
Dean, The University of Texas
Health Science Center at Houston
Graduate School of Biomedical Sciences

**Characterization of Optically Stimulated Luminescent Detectors in Photon &
Proton Beams for Use in Anthropomorphic Phantoms**

A

THESIS

Presented to the Faculty of
The University of Texas
Health Science Center at Houston
and
The University of Texas
M.D. Anderson Cancer Center
Graduate School of Biomedical Sciences
in Partial Fulfillment

of the Requirements

for the Degree of

MASTER OF SCIENCE

By

James R. Kerns, B.S.
Houston, TX

August, 2010

Acknowledgments

I must first thank my advisor Dr. Geoffrey Ibbott for his patience and guidance through my project, as well as my entire committee for their generous contributions and ideas: Dr. David Followill, Dr. Stephen Kry, Dr. Narayan Sahoo, and Dr. Valen Johnson.

Generous thanks must be given to the great minds doing the real research in OSL. I thank Dr. Gabriel Sawakuchi for his patient endurance through all my elementary questions and review of my ideas. I am convinced he will one day solve all the world's problems. As well, Dr. Eduardo Yukihara from Oklahoma State University was a light during darkness, encouraging me during several particularly difficult times, albeit through email, always carrying a positive note. I know the contributions to his field will not soon be forgotten.

I must thank Dr. Paul Jursinic from West Michigan Cancer Center for taking time to indulge me in my quest for data and for sharing his phantom with me. As well, Dr. Cliff Yahnke from Landauer was very helpful in providing connections and information.

Special thanks must go to Jennifer Johnson for all of her encouragement throughout my time as a student. She taught me almost everything I have learned in the clinic, generously allowing me to use her linac, and use it often. Her hard work and commitment to a job well done are aspirations I will strive for in my own career.

Dr. Narayan Sahoo, besides being on my committee, was extremely accommodating in letting me have precious beam time whenever I needed it, and doing so happily. His selflessness and humility are attitudes to be emulated.

Many thanks go to members of the RPC who were essential to my understanding of RPC protocol and assistance with my project: Paola Alvarez, Dr. David Followill, and Dr. Robert Pinney. I've never met a man with as diverse a career as Bob Pinney; his is a life well-lived.

Of course, my classmates were essential in making each day unique and special. All of them have contributed something to who I am and I wish them the best of luck. I must especially thank Sweet Cheeks for her amazing quotes, kind friendship, and laugher at all my jokes and Mr. Z for his infamous gang and encouragement to write my book.

Characterization of Optically Stimulated Luminescent Detectors in Photon & Proton Beams

for Use in Anthropomorphic Phantoms

James R. Kerns, B.S.

Supervisory Professor: Geoffrey S. Ibbott, Ph.D.

This study investigated characteristics of optically stimulated luminescent detectors (OSLDs) in protons, allowing comparison to thermoluminescent detectors, and to be implemented into the Radiological Physics Center's (RPC) remote audit quality assurance program for protons, and for remote anthropomorphic phantom irradiations. The OSLDs used were aluminum oxide (Al_2O_3:C) nanoDots from Landauer, Inc. (Glenwood, Ill.) measuring 10x10x2 mm^3. A square, 20(L)x20(W)x0.5(H) cm^3 piece of solid water was fabricated with pockets to allow OSLDs and TLDs to be irradiated simultaneously and perpendicular to the beam. Irradiations were performed at 5cm depth in photons, and in the center of a 10 cm SOBP in a 200MeV proton beam. Additionally, the Radiological Physics Center's anthropomorphic pelvic phantom was used to test the angular dependence of OSLDs in photons and protons. A cylindrical insert in the phantom allows the dosimeters to be rotated to any angle with a fixed gantry angle. OSLDs were irradiated at 12 angles between 0 and 360 degrees. The OSLDs were read out with a MicroStar reader from Landauer, Inc. Dose response indicates that at angles where the dosimeter is near parallel with the radiation beam response is reduced slightly. Measurements in proton beams do not show significant angular dependence. Post-irradiation fading of OSLDs was studied in proton beams to determine if the fading was different than that of photons. The fading results showed no significant difference from results in photon beams. OSLDs and TLDs are comparable within 3% in photon beams and a correction factor can be posited for proton beams. With angular dependence characteristics defined, OSLDs can be

implemented into multiple-field treatment plans in photons and protons and used in the RPC's

quality assurance program.

Table of Contents

List of Figures

List of Tables

List of Equations

Chapter 1 – Introduction

1.1 Statement of Problem

Quality assurance has always played a critical role in radiation therapy. With the improvement of delivery systems, margins of delivery error have reduced, requiring also that the quality assurance surrounding it improve as well. For a number of decades, thermoluminescent detectors (TLD) have been the passive detector of choice, able to perform in vivo dosimetry as well as remote quality assurance checks of radiation therapy delivery systems (Kirby *et al.* 1986). Because of its long history, TLDs have been well-characterized, making them reliable with relatively small margins of error (Kirby *et al.* 1992). Thermoluminescence (TL) is not without its drawbacks however, including a necessary post-irradiation wait period, energy dependence, careful heating techniques, and destruction of signal after one reading.

In recent years, new materials and methods have been proposed to improve passive dosimetry. One of these includes optically stimulated luminescence (OSL), which is based on the underlying physics phenomena similar to TLDs, but is able to overcome a number of drawbacks inherent to the TLD. However, optically stimulated luminescent detectors (OSLD) have only relatively recently been introduced to medical dosimetry. Thus, it lacks the comprehensive characterization of many mainstream TLD materials. This study aims to characterize OSLDs for use in certain clinical and dosimetric situations relevant to the Radiological Physics Center.

1.2 Radiological Physics Center

The Radiological Physics Center (RPC) is an organization whose mission is to provide consistency in clinical trials involving radiation therapy. Founded in 1968 and funded by the National Cancer Institute, the RPC exists to ensure institutions across the United States subscribe

to a consistent and comparable standard of radiation treatment. This is accomplished in a variety of ways from mailable dosimetry packages to site visits by physicists. Because the RPC must handle over 14,000 beams at more than 1,500 institutions the volume of dosimetry services is quite large. Currently, the mailable dosimetry package consists of an acrylic miniphantom, set up apparatus, and a set of thermoluminescent detectors (Kirby *et al.* 1986). After irradiation, the TLDs are mailed back and read by the RPC to be compared with the institutions stated output. In addition to this remote beam quality assurance via miniphantoms, the RPC has created a number of anthropomorphic phantoms to ensure consistency throughout the treatment delivery process, not just output. These phantoms use the same type of TLD dosimeters. Because of the new developments in OSLD technology, the RPC has begun investigation into other materials for remote dosimetry in miniphantoms and anthropomorphic phantoms.

1.3 Introduction to Optically Stimulated Luminescence Detectors

Optically stimulated luminescence is an increasingly popular method of dosimetry, having been used mainly in personnel dosimetry for over a decade. The material works as a semiconducting dosimeter by releasing light after having been exposed to ionizing radiation. Optically stimulated luminescence was first proposed in 1950s (Antonov-Romanovskii *et al.* 1956) and later as an archeological dating tool in natural minerals (Huntley *et al.* 1985). The phenomenon of OSL is similar to that of thermoluminescence in that ionizing radiation creates electron-hole pairs within the material, stimulating the charges to the valence and conduction bands after which the charges fall into energy traps within the forbidden region, created by defects in the crystal, that prevent immediate recombination. Only upon external stimulation can the charges recombine. The recombination creates excited states of the recombination centers and results in the release of photons in the optical range.

OSLDs have the same possibilities of applications that TLDs do and can thus be used for in vivo, independent, and even real-time dosimetry. The largest difference in the dosimetry process is the readout technique. TLDs are carefully heated while OSLDs are stimulated via optical methods. Optical stimulation can be well controlled quite easily, produced simply and cheaply, and it is possible to achieve a level of certainty comparable or better than TLDs in measurements with the proper techniques (Jursinic 2010a).

Currently, the largest commercial manufacturer of OSLDs is Landauer, Inc. (Glenwood, Ill.) although it is also available as TLD-500 from Harshaw, and only one material is made commercially, aluminum oxide with carbon doping (Al_2O_3:C) although there are other material producers and a number of other materials have and are being tested (Bos 2001; Bulur & Göksu 1998; Yoshimura & Yukihara 2006). Al_2O_3:C was originally designed as a TL dosimeter, noted for its high sensitivity. However, when it was found to be affected by exposure to light, it was investigated as an OSLD (Akselrod & Kortov 1990).

1.4 Proton Therapy

Proton radiation therapy is a rapidly growing form of cancer treatment around the world. Protons were first proposed in the 1940s and treatment began in the 1950s. The first hospital-based proton treatment center was created at Loma Linda University Medical Center, starting treatment in 1990. In 2006, the $130 million University of Texas M.D. Anderson Cancer Center Proton Therapy Center in Houston (PTCH) opened their doors with both passively-scattered and spot-scanning proton beams.

Protons have a unique advantage of treatment over photons. The dose deposition of protons and heavy charged particles (HCP) is higher at the end of the range than at the entrance as shown in Figure 1.1. As well, because protons are charged, the particles have a finite range.

Electromagnetic interactions of the particle with electrons in the medium causes the particle to dissipate energy proportional to the time spent interacting with the medium. Thus, at the end of the range where they have slowed down from numerous smaller interactions, considerably more time is spent interacting with the medium, giving rise to high dose deposition. This energy deposition is related to linear energy transfer (LET). LET is a measure of beam quality, expressed in keV/μm, which describes the rate at which energy is deposited along the particle's track. So for protons, the energy deposition and LET along a given path length increases with decreasing energy. The large energy deposition at the end of the proton range, shown in Figure 1.1 (pristine beam), is termed a Bragg peak, named after its discoverer.
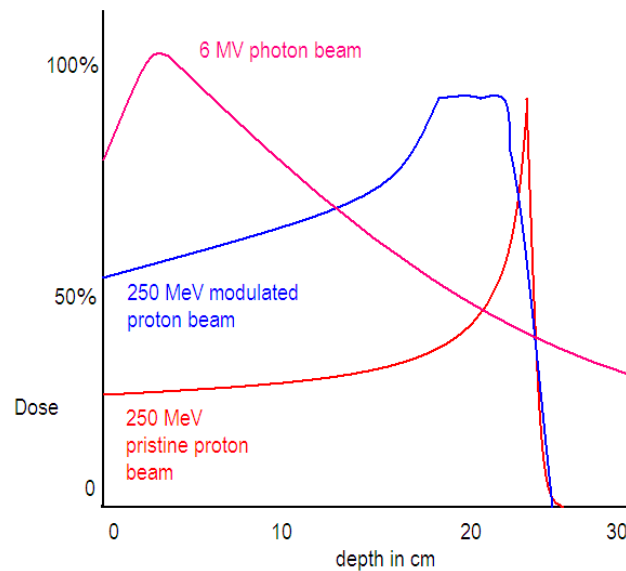
Figure 1.1 The percent depth dose curves for a 6 MV photon beam, and monoenergetic (pristine) and SOBP (modified) proton beams.

Each proton energy has a different penetration depth, or range; thus, to adequately cover an area of interest, a combination of beams with different ranges can be used to create a region of closely grouped Bragg peaks, also called the spread-out Bragg peak (SOBP). The dose within the

SOBP width is approximately uniform as at any given point one portion of protons is at their Bragg peak, shown in Figure 1.1 (modulated beam). One of the methods for combining proton beams with different ranges is by the use of a range modulator wheel which has steps of different thicknesses. During treatment delivery, the wheel spins and protons pass through a track at the edge of the wheel. Because of the spectrum of attenuation thicknesses on the wheel one proton energy can be sent to the gantry with a resulting continuum of proton energies with different ranges causing the formation of the SOBP.

It is important when performing dosimetry with detectors to understand the stopping power of materials. In clinical measurements, we are interested in the dose to the medium at a given point as if the detector were not there. However, we need the detector to be able to determine dose. Density and compositional differences between media and the detectors can differ largely, which must be accounted for in the absorbed dose. Stopping power calculations can account for this difference. Generally, a stopping power can be described as the energy lost per unit path length. Specifically, we define the mass collision stopping power as given in ICRU Report 49 (ICRU 1993):

$$\left(\frac{1}{\rho}\right) S_{col} = \frac{4\pi r_e^2 mc^2}{\beta^2} * \frac{1}{u} * \frac{Z}{A} * z^2 * L(\beta)$$

Equation 1.1 Stopping power equation.

where r_e is the electron radius, mc^2 is the rest energy of an electron, β is the proton relativistic velocity, A and Z are the atomic mass and number of the medium respectively, z is the particle charge number, and $L(\beta)$ is the stopping power number. The stopping power number is a function accounting for small details of the interaction including excitation energy and medium polarization. This stopping power comes into play when determining absorbed-dose energy dependence in protons, discussed further in Section 1.7.2.

Because of the large LET in a proton dose distribution as compared to photons, stopping power plays a large role in determining luminescence of an OSLD. As well, because a proton delivers orders of magnitude more energy than a photon, the total fluence of protons for a given dose is much less than that of photons which causes the dose distribution within the dosimeter to be non-uniform (Sawakuchi *et al.* 2008b).

1.5 OSL Phenomenon

OSL dosimeters function the same way as thermoluminescent detectors in use and application, and derive their properties from the same phenomenon. The phenomenon follows a model of two energy bands, the valence and conduction, separated by a forbidden gap. Defects purposely introduced into the material during fabrication act as local energy bands with levels within the forbidden gap, called traps. When ionizing radiation is introduced to the material it creates electron-hole pairs, and excites electrons up to the conduction band and holes move to the valence band. From here, electrons can travel amongst the crystal lattice until one of two things happen. The electron can cross back towards the valence band and recombine with a hole. However, if near a defect, it can fall into the energy trap. The electron is now prevented from recombining with a hole until it can gain enough energy to once again reach the conduction band. This stimulation is accomplished by either introducing heat, causing TL, or optical photons, causing OSL. The number of trapped electrons is normally proportional to the amount of ionizing radiation received. This is the concept that makes crystals with defects a viable passive dosimeter.

The probability of an electron escaping a trap can be described as a product of stimulation photon flux of a given wavelength, σ, and the photoionization cross-section of the trap, φ, (Akselrod *et al.* 2007), which is shown as:

$$p = \sigma * \varphi$$

Equation 1.2 Photo cross-section equation.

The photoionization cross-section described in Whitley & McKeever (2000) is defined as:

$$\varphi(hv) = a * \left(\frac{\sqrt{E_i} * (hv - E_i)^{\frac{3}{2}}}{hv * (hv - \gamma E_i)^2} \right)$$

Equation 1.3 Photoionization cross-section equation.

where hv represents a stimulation energy greater than E_i, a is a scaling constant, E_i is the optical threshold for a given trap i, and γ represents a function of charge carrier effective mass.

The photoionization cross-section is the most important quantity in predicting stability of a trap when optically stimulated (Bøtter-Jensen *et al.* 2003). The cross-section is determined by the concentration of defects, or traps, and the stimulation energy. Traps have a given energy gap to the conduction band and in order to stimulate the electron the stimulation energy must at least cross this threshold. Models predicting cross-section have been posed, each with a slightly different emphasis on trap level and interaction weighting. The most quoted expressions are those described by Grimmeiss & Ledebo (1975) and Lucovsky (1964) (Bøtter-Jensen *et al.* 2003).

Once an electron escapes a trap it can again fall into a trap or recombine. For simplicity, it can be assumed the electrons do not again fall into more traps and promptly recombine. With this assumption it is possible to describe the luminescence intensity with trapped charges according to:

$$\frac{dn}{dt} = -n * p$$

Equation 1.4 Trap-release and signal decay equation.

Here, $n = n(t)$ is the trapped charge level at time t. With this knowledge an OSLD can be stimulated continuously with a constant photon flux and the resulting light collected to create a signal response intensity curve. Assuming the stimulation is constant and trap numbers are finite, the luminescence and trap charge level, n, should show an exponential decay. The integral of the response curve can be considered proportional to dose. Thus, integrating luminescence of OSLDs irradiated to unknown doses can be used for the dose determination.

Real materials require a more complex model than the ideal one described above due to multiple trapping centers, defect distribution, and charge transfer between traps (Bøtter-Jensen *et al.* 2003). The OSL phenomenon and approach to dosimetry however are based on the basic principles described above.

1.6 Aluminum Oxide with Carbon Doping (Al_2O_3:C)

Aluminum oxide is a clear-to-whitish material grown into crystals in oxygen reducing conditions and carbon presence. For an oxygen vacancy in the lattice, induced during growth, occupancy of the site by one or two electrons can occur, creating either a neutral F-center, or a positively charged center, called an F^+-center. Sensitivity of the crystal is related to the density of F^+-centers, in the range of 10^{15}-10^{16} cm^{-3}, as these are believed to be the points of recombination (McKeever *et al.* 1999). Al_2O_3:C has an effective Z value of 11.28 (Bos 2001). The level of carbon doping can range between 100 and 5000 ppm (Akselrod *et al.* 1993) although the carbon defects developed in growth contribute more to the TL properties than the OSL properties

(Akselrod & Kortov 1990). Aluminum oxide is an extremely sensitive dosimeter, having 40-60 times the TL sensitivity of TLD-100, and is especially suited for OSL applications because the OSL signal is even greater for a given dose than the TL signal (Bøtter-Jensen *et al.* 1997).

One of the most attractive advantages of Al_2O_3:C is the large energy gap of the forbidden region (9.5 eV) (Akselrod *et al.* 2007). This allows defect energy levels to be far enough from the conduction band to reduce normal atmospheric thermal effects.

The electron can fall into a number of different energy level traps. A simple but sufficient explanation of OSL phenomenon can be described by a number of possibilities, shown in Figure 1.2.
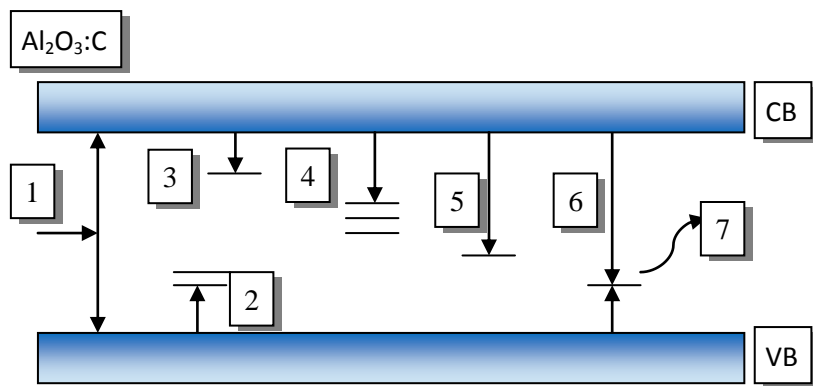
Figure 1.2 Al_2O_3:C phenomenon diagram. The upper block represents the conduction band (CB) while the lower block is the valence band (VB). Each number represents a step or possibility in the OSL process.

In Figure 1.2 the process of OSL is described from creation to luminescence. Process 1 is the creation of an electron-hole pair from exposure to ionizing radiation, where the electron ascends to the conduction band and the hole to the valence band.

In Process 2, once the hole is in the valence band it is free to move about the crystal lattice, where it is possible for it to combine with an F-center to create an F^+-center. There is believed to be some sort of variety of F^+-center energy levels, shown by more than one bar in

Figure 1.2. Hole capture will increase the total possible centers of recombination, described by Equation 1.5:

$$F + h \rightarrow F^+$$
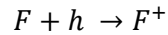
Equation 1.5 F$^+$-center creation from a hole.

Shallow electron traps (SET), represented by Process 3, are quite obviously the traps with the shallowest energy drop from and easiest to stimulate back to the conduction band. Luminescence of shallow traps is observed during and promptly after radiation exposure, thus allowing Al$_2$O$_3$:C to be used for real-time applications (Polf *et al.* 2004; Aznar *et al.* 2004; Andersen *et al.* 2006).

Medium electron traps (MET), represented by Process 4, also called intermediate or dosimetric traps, are deeper than shallow traps and are the trap levels responsible for both the TL and OSL when performing dosimetry. The peak of TL occurs at approximately 200° C which would suggest that the main trap level is stable at room temperature which seems to have been demonstrated in literature (Bøtter-Jensen *et al.* 1997; Homnick 2008). Several trap levels are shown representing the MET since there is a spectrum of stimulation allowable and trap levels responsible for the OSL (Yukihara & McKeever 2006a).

Deep electron traps (DET), represented by Process 5 in Figure 1.2, are ones that are closest to the valence band, meaning it will take a larger amount of energy to stimulate the electron to the conduction band to recombine. The stimulation energy required to release trapped electrons at these levels are mostly beyond the optical range, giving a small stimulation cross-section (see Section 1.5). It is possible to remove all deeply trapped charges by annealing the material to 900° C (Bøtter-Jensen *et al.* 2003). However, Landauer OSLDs are embedded in a plastic casing which would not stand the high temperature. Since the charges that have fallen into

DET are rarely released using optical annealing (bleaching), the total number of available traps lowers. This can cause an increase or decrease in sensitivity over the dose-lifetime of the dosimeter, depending on the deep trap characteristic (Yukihara & McKeever 2006b; Yukihara *et al.* 2003; Yukihara *et al.* 2004).

When the electron drops from the conduction band, either being stimulated from ionizing radiation or from optical stimulation, and recombines with an F^+-center, shown as Process 6, it creates an excited state, F^*:

$$F^+ + e^- \rightarrow F^*$$
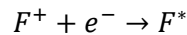
Equation 1.6 F^+-center combination with an electron forming an excited F state, F^*.

After being promoted to an excited state, the dominant emission of the F^+-center is a photon centered around 410-420 nm with a FWHM of 40-50 nm (Yukihara & McKeever 2006a; Markey *et al.* 1995), shown in Figure 1.2 as Process 7:

$$F^* \rightarrow F + h\nu_{420}$$
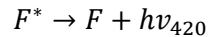
Equation 1.7 Excited F^+-center emission.

This emission of blue light is the largest contributor of signal when using Al_2O_3:C for passive OSL dosimetry using simple readout techniques. However, there is at least one other emission band, an ultraviolet emission, at 335 nm that can be separately detected using certain filters or timing techniques (Yukihara & McKeever 2006a). The emission is thought to be a result of deep hole trap recombination, although the causes are not definite. The emission is more pronounced for high ionization densities, i.e. higher low-LET doses and also for HCP irradiations. As well, the OSL from the UV emission increases with time post-irradiation

(Yukihara & McKeever 2006a). The UV emission is not specifically studied in this work but is important to remember for certain HCP dosimetry systems.

1.7 Relative Luminescence Efficiency

In a luminescence dosimeter the light emitted by the dosimeter is a surrogate for the energy absorbed by the material, usually proportional to the dose absorbed. The RPC compares dose received in a particular radiation field to that of cobalt-60 for reference. Thus, understanding the relation of luminescence efficiency between the reference and a beam quality other than the reference, or the relative luminescence efficiency (RLE), is critical. For OSL, luminescence is largely a function of the dose distribution.

There are two factors responsible for changes in RLE: intrinsic energy dependence and absorbed-dose energy dependence. Intrinsic energy dependence is the relation of a detector's luminescence to the dose received for different energy radiation fields. Absorbed-dose energy dependence is the relation of the dose absorbed by the detector to that of the reference medium, dependent on the mass energy absorption coefficient in photon irradiations and on the LET in HCP irradiations.

The response of synthetic sapphire, Al_2O_3:C, to photons can be predicted using basic knowledge about the detector's elemental composition. The attenuation coefficient, absorbed-energy, etc. of each element can be determined in photons and the combination used for material response prediction. In general, for a luminescent dosimeter, the luminescence efficiency, η, in a radiation field, f, is the ratio of luminescence from the detector, L_f, to the medium's absorbed dose, D_f:

$$\eta_f = \frac{L_f}{D_f}$$

Equation 1.8 Relative luminescence definition.

The luminescence defined here is understood to be the light collected by the dosimeter's reader. This collection is highly dependent on the reader and geometry used, but if the same reader is used for all measurements then this variable is removed.

It follows then that the RLE of a detector type in a given radiation field is the ratio of the luminescence efficiency in one radiation field to that of another. Since the RPC references doses to muscle in cobalt-60, an RLE equation can be derived for any radiation field, f, in a given medium, m:

$$\eta_{f,Co60}^m = \frac{\eta_f^m}{\eta_{Co60}^m}$$

Equation 1.9 RLE defined for a radiation field referenced to cobalt-60.

Notice that the RLE is similar in nature to the beam quality conversion factor, k_Q, used in ion chamber dosimetry calibration (Almond *et al.* 1999; Andreo *et al.* 2000). The absorbed dose in the medium must be found relative to the dose calculation reference medium, in this case water, w. This can be defined as:

$$D_{Co60}^{m,w} = \frac{D_{Co60}^{medium}}{D_{Co60}^{water}}$$

Equation 1.10 Absorbed-dose definition related to a reference medium for cobalt-60.

One major reason that luminescence efficiency ratios develop is because absorbed doses to the dosimeter in the reference beam and beam quality f vary for the same delivered dose to the

mediums. In all of the equations, it is assumed that the same fluence dose is delivered; were it

not, the RLE would have to be corrected by a delivered dose ratio.

1.7.1 Photon Relative Luminescence Efficiency

From Equation 1.9 and Equation 1.10 we can define the luminescence efficiency of

Al$_2$O$_3$:C for photon fields in terms of absolute luminescence, absorbed dose, and mass-energy

absorption coefficients:

$$\eta_{f,Co60}^{Al2O3} = \frac{\dfrac{L_f^{Al2O3}}{D_f^{Al2O3,w}}}{\dfrac{L_{Co60}^{Al2O3}}{D_{Co60}^{Al2O3,w}}} = \frac{\dfrac{L_f^{Al2O3}}{\left(\dfrac{\mu_{en}}{\rho}\right)_f^{Al2O3,w}}}{\dfrac{L_{Co60}^{Al2O3}}{\left(\dfrac{\mu_{en}}{\rho}\right)_{Co60}^{Al2O3,w}}}$$

Equation 1.11 RLE for a photon field referenced to cobalt-60 and dose to water.

where *D* is the absorbed dose to aluminum oxide relative to water which is assumed to be

proportional to the mass-energy absorption coefficient, μ_{en}/ρ, for Al$_2$O$_3$ and water. Again, this

assumes the detectors are the same size, read in the same reader, and are both given the same

reference dose.

From here, elemental data taken from the National Institute of Standards and Technology

(NIST) were used to find the mass-energy absorption coefficients for a spectrum of energies

(Hubbell & Seltzer 2004). The data for aluminum and oxygen were combined and weighted

according to mass composition percentage from Bos (2001) and shown in Figure 1.3 Mass

energy-absorption coefficient ratio of aluminum oxide to water for photon energies 10 keV to 20

MeV.. This shows the mass-energy absorption coefficient for Al$_2$O$_3$ across the photon spectrum

10 keV to 20 MeV. It can be seen the detector largely over-responds relative to water at diagnostic energies compared to the MV range, but does not show large changes above 200 keV. The response at low energies has been seen experimentally and agrees with absorbed dose calculations (Reft 2009; Bos 2001). Table 1.1 Quality dependence factors for select photon energies based on NIST absorbed-dose and MC calculations of Mobit et al. (2006). shows a short list of mass-energy absorption coefficients for select energies that have been normalized to cobalt-60, also referred to as the quality dependence factor. For 6 MV photons, the average photon energy is $\approx$1/3 of the accelerating potential. So, for a 6 MV photon beam, attenuation values predict a negligible response increase, and a 3-4% increase at 15 MV. Response values should be determined experimentally however to confirm predictions.

Linac Energy (MV)	Effective Energy (MeV)	NIST Al_2O_3 / water μ_{en}/ρ	Mobit et al. (2006)
Co-60	1.25	1	1
6	$\approx$2	1.003	0.99±0.3%
15	$\approx$4	1.035	0.98±0.3%

Table 1.1 Quality dependence factors for select photon energies based on NIST absorbed-dose and MC calculations of Mobit et al. (2006).

Predictions using Monte Carlo (MC) simulations were done by Mobit *et al.* (2006), shown in Table 1.1 and determined that response was approximately independent of energy between Co-60 and 6 MV photons, with a decrease in relative response of $\approx$2% in 15 MV photons. Chen *et al.* (2009) used another MC simulation to determine absorbed dose to Al_2O_3:C dosimeters, concluding with similar results. The quality conversion factor, determined as the absorbed dose ratio of Al_2O_3:C to water for cobalt-60 compared to linac MV spectra from 6-24 MV, was determined to be 0.995±1%. Thus, experiments in this study should expect little difference between cobalt-60 and MV signal response.
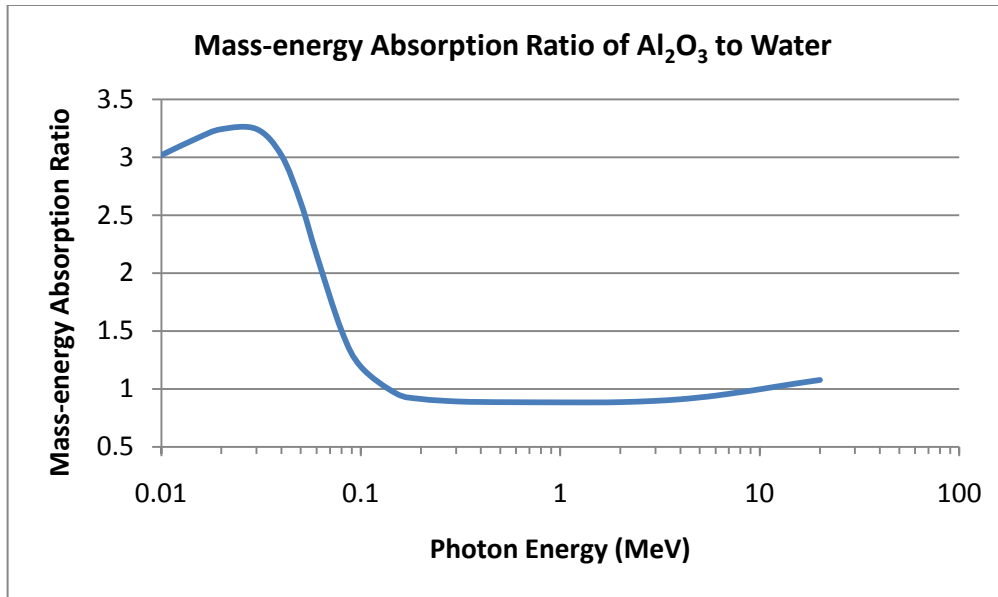
Figure 1.3 Mass energy-absorption coefficient ratio of aluminum oxide to water for photon energies 10 keV to 20 MeV.

1.7.2 Heavy Charged Particle Relative Luminescence Efficiency

It was a goal of this study to determine the relative luminescence efficiency of Al_2O_3:C in selected proton beams for the dosimetry system of the RPC. The efficiency of aluminum oxide in high energy HCPs has been extensively covered by Sawakuchi *et al.* (2008a), wherein the appendix defines general RLE for HCPs, although the dosimetry system was different than the one used in this study. Relative luminescence efficiency will be defined by the dose absorbed by the medium relative to water, just as for photons. For charged particles, Equation 1.11 is modified appropriately:

$$\eta_{HCP,Co60}^{Al2O3} = \frac{\dfrac{L_{HCP}^{Al2O3}}{D_{HCP}^{Al2O3,w}}}{\dfrac{L_{Co60}^{Al2O3}}{D_{Co60}^{Al2O3,w}}} = \frac{\dfrac{L_{HCP}^{Al2O3}}{S^{Al2O3,w}}\Big/ \rho_{HCP}}{\dfrac{L_{Co60}^{Al2O3}}{\dfrac{\mu_{en}}{\rho}^{Al2O3,w}}\Bigg|_{Co60}}$$

Equation 1.12 RLE for a proton field referenced to cobalt-60.

where now the relative absorbed dose in charged particles is dependent on the mass stopping power ratio of aluminum oxide to water. Figure 1.4 shows the stopping power of aluminum oxide relative to water for a spectrum of energies in protons, taken from the NIST PSTAR data (Berger *et al.* 2005). Table 1.2 shows a short list of stopping powers of Al_2O_3 and Al_2O_3 relative to water for select nominal proton energies. For low doses of relatively low LET (photons and therapeutic proton energies) the absorbed dose can be assumed to be in the linear response region of the dosimeter (Sawakuchi *et al.* 2008a), although this does not always hold true for higher low-LET doses and for heavy ions (see Section 2.3.3 & 2.3.4).
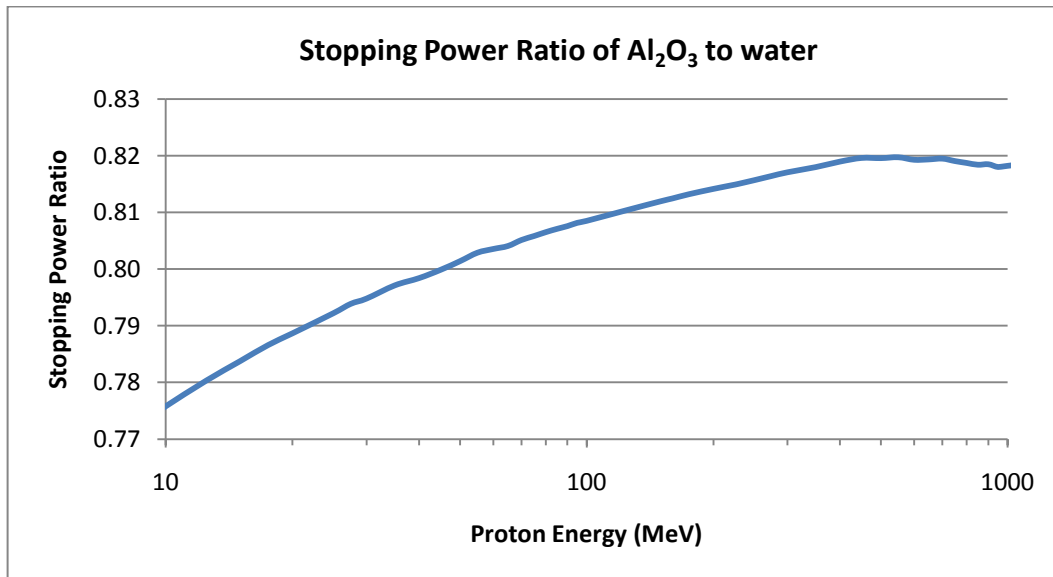
Figure 1.4 Stopping power ratio of aluminum oxide to water for the spectrum of proton energies 10 to 1000 MeV.

Energy (MeV)	Al₂O₃ S/ρ (MeV cm²/g)	Al₂O₃/water S/ρ ratio	Al₂O₃ Proton/ Co-60 Absorbed Dose Ratio
70	7.696	0.805	0.911
100	5.893	0.808	0.915
160	4.232	0.812	0.919
200	3.657	0.814	0.921
250	3.190	0.816	0.923

Table 1.2 Mass stopping powers and ratios for select proton energies.

As an example, the relative luminescence efficiency of 250 MeV protons can be calculated as follows. According to the NIST X-ray coefficient data, the dose absorbed by Al_2O_3:C when irradiated by cobalt-60 to 1 Gy in water is 88.4%, or 0.884 Gy. The dose absorbed by Al_2O_3:C in 250 MeV protons of 1 Gy relative to water is 81.4%, or 0.816 Gy. Recall that doses for RLE calculation are relative to water as it is the reference medium. So, according to the absorbed-dose and *ceteris paribus*, the predicted relative luminescence efficiency of Al_2O_3:C of 250 MeV protons to Co-60 is:

$$\eta_{H250MeV,Co60}^{Al2O3} = \frac{\frac{L_{H250MeV}^{Al2O3}}{\frac{S^{Al2O3,w}}{\rho}_{HCP}}}{\frac{L_{Co60}^{Al2O3}}{\frac{\mu_{en}}{\rho}^{Al2O3,w}_{Co60}}} = \frac{\frac{L_{H250MeV}^{Al2O3}}{0.816}}{\frac{L_{Co60}^{Al2O3}}{0.884}} = \frac{L_{H250MeV}^{Al2O3} * 1.083}{L_{Co60}^{Al2O3}} \rightarrow L_{Co60}^{Al2O3} = L_{H250MeV}^{Al2O3} * 1.083$$

Equation 1.13 RLE defined for 250 MeV protons relative to cobalt-60.

The above equation says that according to absorbed dose, the RLE of Al_2O_3:C in cobalt-60 is 1.083 times greater than that in 250 MeV protons for the same reference dose. Thus, according to the absorbed-dose RLE calculation, our example of an irradiation of Al_2O_3:C in 250 MeV protons to 1 Gy would show a signal upon readout of around 0.923 Gy relative to cobalt-60.

In going from the left side of the arrow to the right in Equation 1.13 we have assumed that the response of dose in the OSLD is linear, which is safe for low doses (Sawakuchi *et al.* 2008a; Yukihara & McKeever 2006b).

The values given as doses to the two mediums are the absorbed-dose energy dependencies, or the difference of absorbed dose between the detector and the reference medium *sans* the detector. Any intrinsic energy dependence would be the difference between the expected luminescence (0.923 Gy in our example) and the measured luminescence. It is predicted then that according to the absorbed dose the RLE will show a degree of under response in protons compared to Co-60.

The predictions listed in Table 1.2 are for the nominal energies of the beam, not the clinically relevant region (SOBP), which was the area of interest of this study and is for therapeutic assessment. The LET at the surface of the medium, corresponding as well to the nominal energy, is much lower than that at the Bragg peak or the SOBP. Because the SOBP is a continuum of proton energies the true LET is difficult to determine. In this study both the nominal energy and approximate LET at the dosimeter location were used in discussion of energy dependence.

1.8 OSL Dosimetry

The basic process of inducing and capturing luminescence in OSL dosimetry is shown in Figure 1.5. The process starts with a source of light, i.e. stimulation, usually from a light-emitting diode (LED) or laser, possibly passing through a band-pass filter to select the desired wavelengths. The stimulation photons then impinge on the dosimeter, bringing about the recombination discussed in Section 1.6. After recombination the emission photons as well as stimulation photons enter through another filter to block the stimulation photons from entering

19

the last stage of dosimetry, the photomultiplier tube (PMT) where the photons are multiplied and then electronically counted. This is the basic concept behind OSL dosimetry but results can be achieved through a variety of methods.
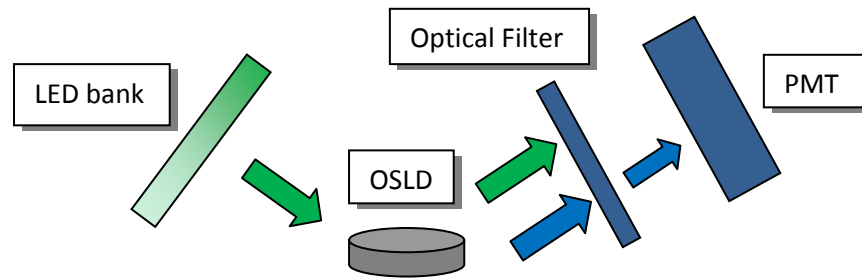
Figure 1.5 Schematic of OSL readout system.

The easiest way to read an OSLD is to simply turn on the stimulation LEDs for a set time and then simultaneously collect recombination photons with the PMT. This process is called continuous-wave OSL (CW-OSL) and is simple in practice and provides reliable results. Normally, it takes a few minutes to stimulate all the charges in the dosimeter. Initial intensity of the decay curve can also be used to determine dose, meaning a short exposure to stimulation can give somewhat similar information as the entire decay curve. However, initial intensity is not always proportional to the integral of the decay curve. In low-dose situations (<1 Gy), dose affects how fast the signal decays and thus area of the curve. As well, LET affects the decay curve and initial intensity because of the concentrated dose distribution of the depositing particles. Studies in relativistic ion beams show that initial intensity increases proportionally to the curve integral with increasing LET (Yukihara *et al.* 2004).

Another readout method uses timed pulses of LED light, stimulating the dosimeter for a short time, turning off the LED stimulation, then immediately and briefly afterward collecting the recombination photons, a process called pulsed-OSL (POSL) (Akselrod & McKeever 1999). The

process can make time-resolved measurements which capture only F^+-center emissions due to the long half-life relative to the UV emission (Yukihara & McKeever 2006a).

Presently, the only widely available commercial OSL dosimetry system is the Landauer MicroStar reader and has been addressed and used several times in literature (Jursinic 2007; Jursinic 2010a; Viamonte *et al.* 2008; Reft 2009). This system incorporates the initial intensity CW-OSL process and was the reader used in this work.

A research reader with a high level of precision is the Risø OSL/TL reader (Risø National Laboratory, Denmark). This system is automated and can accommodate different filters and types of stimulation as well as a calibrated beta radiation source that eliminates differences in individual dosimeter sensitivity, accumulated dose, and reader sensitivity, and environmental effects (Yukihara *et al.* 2005). This system can use CW-OSL or POSL. A number of OSLD characteristics have been found using this reader.

1.9 Thermoluminescent Dosimeters

The current standard of the RPC's mailable dosimeter program is the thermoluminescent dosimeter. This dosimeter has been in use for a number of decades and a number of applicable materials have been characterized to high levels of precision. The protocol used by the RPC for reading and correcting dose is fully described in Kirby *et al.* (1986) and is briefly summarized here. The RPC uses TLD-100, Lithium Fluoride (LiF), in the miniphantom dosimetry as well as the anthropomorphic phantom program. The trapped charge phenomenon is very similar to that of OSLDs described in Section 1.5. The powder is packaged in polystyrene cylindrical capsules holding about 20 mg of TLD powder.

TLD-100 has been well-characterized by the RPC, of which the correction factors are determined for every incoming powder batch to determine uncertainty (Kirby *et al.* 1992). Before being used for remote dosimetry, the correction factors for energy, dose linearity, back-scatter, and post-irradiation fading must be determined, discussed in Section 2.3.

1.10   Hypothesis & Specific Aims

Because of a number of key advantages over TLDs, OSLDs are gaining popularity in passive dosimetry. Yet, there is much to be known about OSLDs and more research needs to be done to allow them to reach their full potential. This study aims to characterize OSLDs for the RPC's OSL dosimetry system.

The Radiological Physics Center exists to ensure that cancer centers participating in clinical trials deliver radiation therapy doses that are consistent and comparable to each other. The current system of comparison uses mailable TLD packages and the results are compared with the institution's stated output. However, with the potential of OSLDs, the current system could be converted to this new technology to give equivalent, if not better, results at lower cost, hence the drive to fully characterize them (Homnick 2008).

The hypothesis of this study was: *OSLDs can be used to measure dose in both photon and proton beams with accuracy that is within 3% of TLD response and can be characterized in full-phantom conditions.*

The specific aims of this study were:

-Determination of the dose responses and reproducibility of OSLDs in photon and proton beams.

The RPC must maintain a high level of reproducibility and the OSL dosimeter must be able to reproduce signal consistently. OSLDs and TLDs will be irradiated simultaneously to 100cGy in cobalt-60 and 6MV photons and in protons at clinical energies in the spread-out Bragg peak and the responses referenced to cobalt-60 to determine energy dependence values as well as determine reproducibility.

-Determination of OSLD signal fading post-irradiation with proton beams.

Because of a different dose distribution, the OSLD signal fading in protons could be different than photons, thus the response of the dosimeter was studied for various times post-irradiation. This was done by irradiating groups of dosimeters in protons at predetermined times and then reading them all out at the same time.

-Characterization of the angular dependence of OSLDs in photon & proton beams.

Angular response is important for multi-field treatments and must be analyzed before the RPC uses them for such cases. OSLDs will be irradiated in the RPC pelvic phantom every 30 degrees relative to the radiation beam to form a 360-degree angular response of the detector.

Chapter 2 – Materials & Methods

2.1 RPC TLD Dosimetry

The dosimetry protocol for TLDs is well established at the Radiological Physics Center. Each batch that the RPC receives is characterized to determine all applicable correction factors for the irradiation systems that will be tested. For the TLDs, the following equation is used to determine absolute dose D from raw readings relative to an institution's reference situation, drawn from Kirby *et al.* (1986):

$$D = Reading * S * K_l * K_f * K_e * B * I * ddf$$

Equation 2.1 TLD dose calculation from a reference point.

where *Reading* is the thermoluminescence reading, or signal, divided by the mass of the powder, S is the system sensitivity factor, described later in Section 2.2.1, K_l is the dose linearity factor, K_f is the post-irradiation fading factor, K_e is the energy correction factor, B is the backscatter factor, I is the inverse-square correction, and *ddf* is the depth dose factor (percent depth dose, tissue maximum ratio, etc). These factors are curve-fitted from the characterization data collected by the RPC for each TLD batch received.

The calculation used for determining dose in an experimental situation, i.e. not from a reference point, can be drawn by removing the reference factors from Equation 2.1:

$$D = Reading * S * K_l * K_f * K_e$$

Equation 2.2 TLD experimental dose calculation.

with all other factors keeping the same definition as Equation 2.1.

The post-irradiation fading of TLDs for the batch used in this study is corrected at the RPC by the following equation:

$$K_f = \frac{N}{a * e^{-b*x} + c * e^{-d*x}}$$

Equation 2.3 TLD fading factor.

with constants $N = 1.3493$, $a = 1.2815$, $b = 0.00010885$, $c = 0.06781$, $d = 0.071908$, and x being the number of days since irradiation. The double exponential is a curve-fitting model based on empirical data. TLDs are not normally read earlier than 10 days post-irradiation to minimize thermal effects of traps that affect the luminescence.

Energy dependence factors for the RPC have been tabulated by photon and electron energies. Photon factors relevant for this study are cobalt-60 = 1 and 6 MV = 1.03. For protons, an energy correction factor of 1.000 is used, although proton data acquired through the RPC's remote auditing has a observed a spectrum of results differing approximately ±2% from unity (Ibbott *et al.* 2008).

The linearity of dose from the range 0.2 Gy to 6 Gy is determined from the following equation:

$$K_l = m * raw\ dose + b$$

Equation 2.4 TLD linearity factor.

where the constants $m = -0.00028943$ and $b = 1.08683$. Raw dose is defined as:

$$raw\ dose = Reading * S * K_f$$

Equation 2.5 TLD raw dose calculation.

where *Reading*, *S* and K_f are the same as in Equation 2.1, representing the TL reading, system sensitivity, and the fading correction.

2.2 RPC OSL Dosimetry

With the development of usable OSL materials, a considerable number of papers have described the characteristics of the materials and tested reader systems, creating a rapidly growing knowledge base. The RPC regards OSL dosimetry worth pursuing and has worked to create a dependable protocol. For part of this study, OSLDs and TLDs were irradiated simultaneously in cobalt-60 beams, 6 MV photon beams, and 200 MeV proton beams for comparison and to determine the relative response of the OSLD using the RPC dosimetry protocol.

To determine OSL absolute dose several correction factors must be applied to the raw readings. The following proposed equation was derived from the Kirby *et al.* (1986) definition to determine absolute dose in OSL dosimetry relative to a reference situation:

$$D = Reading * ECF * C_f * C_l * C_e * C_d * S * B * I * ddf$$

Equation 2.6 OSL dose calculation from a reference point.

In Equation 2.6 *Reading* is the raw PMT counts obtained when reading the dosimeter. *ECF* is the individual element correction factor, discussed in Section 2.2.2. C_f is the correction factor for signal fading post-irradiation, C_l is the linearity correction factor, C_e is the energy dependence factor, and C_d is the read-out depletion factor. The variables *B*, *I*, and *ddf* hold the

same meaning as in Equation 2.1 for backscatter, inverse-square, and depth-dose factors. The effects of these factors are discussed in Section 2.3. Finally, S is the system sensitivity factor that converts counts to dose, discussed in the following section. To calculate dose in an experimental situation, i.e. not from a reference point, Equation 2.6 can be reduced to the following:

$$D = Reading * ECF * C_f * C_l * C_e * C_d * S$$

Equation 2.7 OSL experimental dose calculation.

All the variables hold the same definitions as before. This was the equation used to determine dose in all the OSL experiments in this study.

2.2.1   System Sensitivity Factor

All OSLD and TLD readings must be converted to absolute dose. To accomplish this, precise measurements of received dose must be obtained. The RPC achieves this by irradiating dosimeters to known doses in cobalt-60, referred to as "standards", which when read create a sensitivity factor. Sets of standards are irradiated in custom acrylic miniphantoms which are placed on a jig attached to the cobalt machine. The field is set to 10x10 cm^2; the platform is perpendicular to the beam and set to 80 cm SSD. The miniphantom sits atop the platform; the phantom is 1.5 cm thick with the dosimeters in the center, putting them at 79.25 cm from the cobalt source. The dosimeters are then irradiated to a known dose. The cobalt source was calibrated following TG-51 protocol (Almond *et al.* 1999) in water but the dose must be calculated to the location of the dosimeters. This dose rate must be decay-corrected from the time of calibration, converted to dose in air, and inverse-square corrected. These standards are read at the beginning and end of a session to create a sensitivity value and ensure stability of the reader during the reader session.

2.2.2   Element Correction Factor

An element correction factor (ECF) is simply a term used to describe and correct for sensitivity of an individual OSL dosimeter. In production, a number of grown Al_2O_3:C crystals are mixed together to create larger batches of similar uniformity in sensitivity. However, because of the inherent heterogeneity of traps in crystal growth, sensitivity is still varied within the batch of dosimeters. At the RPC, to reduce uncertainty in the dosimetry, a large group of dosimeters is irradiated to a small amount of known dose in cobalt-60 and then read out to determine sensitivity of the dosimeter. The response of an individual dosimeter is compared to the average of the group reading and from the ratio a correction factor is determined. After obtaining the ECF, it is applied to the raw readings of the dosimeter in subsequent uses as per Equation 2.7. It is important to note that the sensitivity of the dosimeter is known to change with accumulated dose (see Section 2.3.4). Because OSLDs at the RPC are not used after obtaining a history of 10 Gy accumulated dose no sensitivity correction is needed; i.e. only one ECF is needed for the lifetime of the dosimeter.

2.2.3   NanoDot OSL Dosimeter

The OSLDs used in this study were the newest generation of InLight/OSL commercial dosimeters from Landauer Inc., called the nanoDot. Landauer has created a family of these dosimeters, ranging from the Luxel which is used in personnel monitoring to single Al_2O_3:C crystals to the previous generation InLight dosimeter. The nanoDots measure 1x1x0.2 cm^3 and are pictured in Figure 2.1. The sensitive material is covered in a light-tight black plastic casing when closed, preventing accidental light exposure and thus signal depletion. The plastic casing has a density of 1.03 g/cm^3, and the leaf thickness covering the front and back of the nanoDots is

28

0.36mm (Jursinic 2010a). The actual dosimeter material is a 5 mm diameter white disk made of

Al_2O_3:C 0.2 mm thick with polyester foils on either side, 0.03 mm thick, embedded in the plastic

case (Perks *et al.* 2008). The disk can slide out of the casing for reading and bleaching. Each

dosimeter is printed with a unique serial number to allow tracking by both the manufacturer and

client user.

Dosimeters are created in batches. Al_2O_3 crystals are grown in an oxygen deficiency and

doped with carbon, up to 500 ppm (Bøtter-Jensen *et al.* 2003). Multiple crystals are then crushed

and mixed together to provide better uniformity across the batch (Perks *et al.* 2007). In batches

meant for the RPC, 95% of the dosimeters must have an individual sensitivity within 5% of the

batch average sensitivity or they are thrown out to meet the requirement.
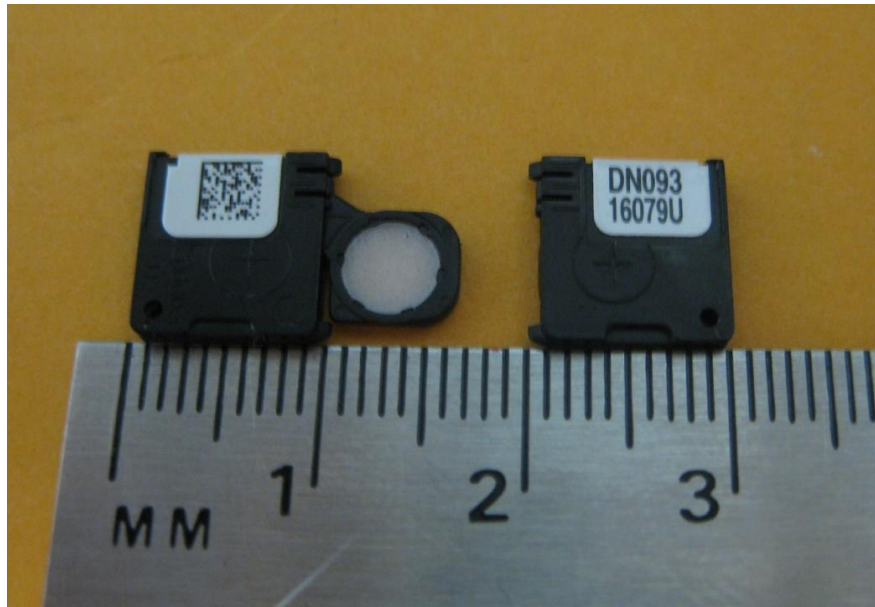
Figure 2.1 NanoDot OSLD.

2.2.4   MicroStar Reader

The microStar reader, shown in Figure 2.2, is another product of Landauer and is currently used by the RPC to read OSLDs. The reader consists of a drawer to insert OSLDs, shown in Figure 2.3, where they are opened and an array of LEDs stimulates the dosimeter and a PMT collects the resulting stimulation light. This is the process shown in Figure 1.5. Software used in conjunction with the reader allows results to be displayed and also tracked in a database that can be exported to an Excel spreadsheet for further analysis. While options exist to allow the user to enter certain parameters to calculate final dose, only the PMT counts were recorded for this study with the absolute dose calculation done later in accordance with RPC protocol and correction factors.

Figure 2.2 MicroStar reader with accompanying computer with microStar software.

Figure 2.3 MicroStar reader with drawer extended showing the OSLD insert area.

Figure 2.4 MicroStar knob control allowing selection of QA measurements or dosimeter readout.

The process to read a group of dosimeters consists of a number of steps. First, the

dosimeter barcode must be scanned or the serial number manually entered prior to reading. The

dosimeter is then inserted into an adapter designed to hold and open the nanoDot and then placed in the reader drawer and closed, shown in Figure 2.3. The readout knob is then turned from the "Home" position to "E1" to start the readout process, shown in Figure 2.4. Normally, the reader is set to stimulate the dosimeter for $\approx$1 second, but for RPC dosimetry and this study the time is set for 7 seconds for better statistics. At the end of the readout time the number of PMT counts are displayed via the microStar software and logged in a database. The OSLD is removed from the drawer and the reader is set to accept another dosimeter.

The luminescence that enters the PMT must be filtered to remove stimulation photons. The microStar reader model used in this work has two band-pass filters: a Hoya B-370 and a Schott BG-12. The transmittance of these filters is shown in Figure 2.5. Both of these filters start transmittance at approximately 300 nm. The Hoya filter transmittance peaks at 370 nm, while the Schott does so at 400 nm. Notice that in theory this means that at least partial collection of both the F^+-center emission (420 nm) and UV emission (335 nm) is possible. As well, the LED stimulation light is shown in Figure 2.5 in arbitrary units with a wavelength peak at 532 nm (Perks *et al.* 2008).
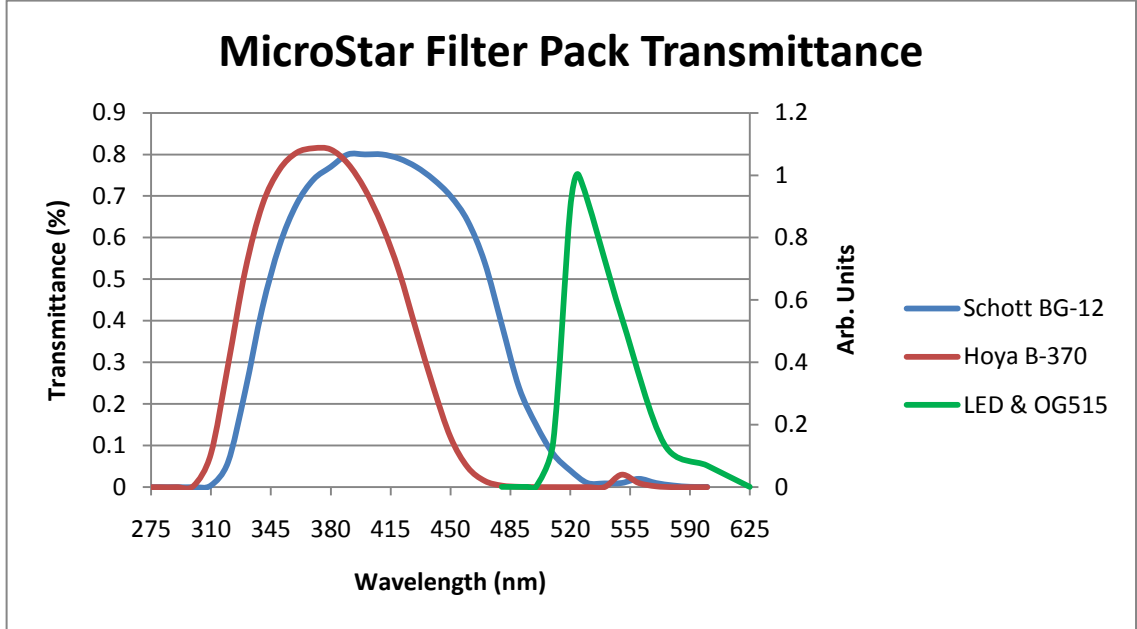
Figure 2.5 MicroStar OSL filter transmittance and LED stimulation light.

Some measure of quality control (QC) of the reader can be accomplished within the software. Before a reading session the reader knob can be turned to different positions to measure inherent aspects of the reader, shown in Figure 2.4. One setting, DRK, measures the dark current (electrical noise) of the system; another, CAL, measures the response of the PMT to a ^{14}C source within the reader; the last, LED, is a reading of the counts recorded with the LEDs turned on. The counts produced by the LEDs and electrical noise are both quite small.

Each session was started by letting the reader warm up for at least a half hour. The reader was then tested to measure the dark current, calibration source, and LED counts to ensure system stability over several readings as well as compared to previous reading sessions. Two sets of two OSLD standards were then read, followed by the experimental OSLDs, then two more standards measured at the end of the session. If reading a large group of dosimeters, standards were read within the session after reading a portion of experimental OSLDs.

2.3 OSLD Characteristics

There are a number of advantages of OSLDs, however, it must be noted that some of them are characteristics of the crystal itself (Al_2O_3:C). Not only is aluminum oxide sensitive as a TL detector but even more so for OSL. However, since OSLDs are a relatively new dosimeter, there is less literature about them than other TLDs and TLD materials.

Beyond the advantageous characteristics of Al_2O_3:C and the OSL phenomenon, there are a number of other characteristics that must be accounted for when read out. Temperature, linearity, energy dependence, linear energy transfer (LET) dependence, angular dependence and fading are all factors studied in full or part by previous work and do or could have an effect on response.

2.3.1 Environmental Effects

Even though theoretically the crystal should be independent of environmental effects, it is important to evaluate it. Physically, temperature could have an effect on the dosimeter causing shallow traps to recombine and thus reducing read out signal. Studies show little ($\leq 1\%$) if any dependence of Al_2O_3:C OSLDs to irradiation temperature, humidity in storage, or storage temperature (Jursinic 2007; Homnick 2008; Miller & Murphy 2006; Yukihara & McKeever 2008). It can thus be presumed from the initial data that environmental effects are unity for clinical situations and thus do not need to be included in the dose equation.

2.3.2 Energy Dependence

Energy dependence of Al_2O_3:C, C_e, has been studied in a number of works and results are varied. Mobit *et al.* (2006) performed Monte Carlo calculations of the response of Al_2O_3:C showing up to a 2% difference between cobalt-60 and high energy photons, shown in Table 1.1. Studies using the Risø OSL/TL reader indicate differences of 0.51±0.48% between 6 and 18 MV photons (Yukihara *et al.* 2008b). Schembri & Heijmen (2007) found a difference of approximately 4% between 6 and 18 MV photon beams; the discrepancy is not clear. Other studies using the MicroStar reader show interesting results. Jursinic (2007) found no energy dependence between 6 and 15 MV photon beams within experimental uncertainty. Viamonte *et al.* (2008) found similar results for 6 and 18 MV beams; however, there was a clear difference in response to cobalt-60 compared to MV beams of approximately 4%. Again, the cause of difference is not clear.

It should be noted that for diagnostic x-ray energies and radioactive nuclear sources the response of Al_2O_3:C is increased significantly, predicted by absorbed-dose in Figure 1.3 (Mobit *et al.* 2006; Reft 2009; Jursinic 2007). This is due to the relatively high Z value of Al_2O_3, prompting more photoelectric photon interactions.

2.3.3   LET Dependence

Along the same lines as energy dependence, Al_2O_3:C shows LET dependence in HCPs and a full discussion is stated in Section 1.7.2. Changes in signal become pronounced with increasing LET. The difference in response, although caused by the deposition of dose of HCPs dependent on energy of the particle at the point of interest, will be assimilated in our nomenclature with the energy dependence factor, C_e. Studies show that signal response drops with increasing LET over the range of high-energy HCPs especially for relativistic ions (Gaza *et al.* 2004; Yukihara *et al.* 2006, Sawakuchi *et al.* 2008a). Studies within therapeutic energy proton

beams show reduced efficiency at the end of a pristine proton beam range (Yukihara *et al.* 2010). This is due to the increase in LET of the beam inducing saturation of local traps within the detector material. Measurements of luminescence with very high ionization density inside Al_2O_3:C using low-LET beta irradiation can demonstrate the response of the detector when the traps become saturated as was demonstrated by Yukihara & McKeever (2006). The results from these studies can create an approximation of response for OSLDs in proton beams.

2.3.4   Linearity

What is referred to as linearity of OSLDs can be described in two terms, which describe two closely related but distinct phenomena. The first is the linearity of the dosimeter response with single dose irradiation. The relative response of Al_2O_3:C to dose seems to show linearity dependence much like TLDs. Yukihara *et al.* (2008) using the Risø OSL/TL reader showed linearity with dose up to 1 Gy, with supralinearity observed above 1 Gy up to a few hundred Gy. This can be modeled as deep traps in the lattice getting filled but because of the large energy gap the DET captured charges are rarely stimulated again to recombine because of its small cross-section (see Section 1.5). As more DETs get filled with increasing dose, more shallow and dosimetric traps capture the charge. This modifies the response to set doses and should to be accounted for in applicable situations. Each dosimetry system used can have different findings for linearity depending on filters and luminescence collection method and so calibration of each system is strongly recommended. This is the effect accounted for in the linearity correction factor C_l in OSLDs. Both experimental and standards irradiations in this study were never over 1 Gy, thus removing the need for a dose linearity correction.

The second term describing linearity is the sensitivity, which is the signal response per unit dose across accumulated dose. Previous work (Jursinic 2007; Homnick 2008) showed that,

using the same model reader used in this work, dosimeter sensitivity is stable up to approximately 20 Gy. It is important to realize that the difference between this sensitivity and supralinearity discussed earlier is the dose per irradiation. The supralinearity observed and noted above is for single-dose measurements, where dosimeters are irradiated once to a specific dose and read out. Jursinic irradiated OSLDs to 1 Gy, read them, bleached, and irradiated again, measuring the sensitivity for each 1 Gy irradiation to test for changes in the sensitivity caused by the dose history. For doses above 20 Gy, the sensitivity is known to diminish (Jursinic 2007), although certain calibration procedures can eliminate this factor entirely (Yukihara *et al.* 2005). Jursinic (2010a) studied accumulated dose using nanoDots and proposed a method to solve for accumulated dose effects in Al_2O_3:C, allowing use to doses over 100 Gy, but the method has yet to be tested. In both the RPC protocol and this study, dosimeters with more than 10 Gy accumulated dose were not used, and thus no sensitivity correction was used. If new data better describes the sensitivity of OSLDs for doses below 20 Gy a correction factor could be implemented.

2.3.5 Fading

Post-irradiation fading is a characteristic inherent to both TLDs and OSLDs, corrected for by C_f. It is theorized that some of the electrons in the shallow traps of the crystal can be excited to the conduction band with room temperature thermal energy and thus recombine soon after irradiation. For Al_2O_3:C, the first 15-20 minutes following irradiation seems to show a short-term exponential drop in signal, with a half-life of roughly 0.8 minutes (Jursinic 2007). Longer-term fading seems to be present, with a drop of 2-3% after the first 5 days after irradiation (Viamonte *et al.* 2008). One study of fading between two weeks and one month post-irradiation showed fading of approximately 2% (Schembri & Heijmen 2007). However, Akselrod *et al.* (1993)

showed no appreciable fading of signal from 1 day to 2 years post-irradiation although

uncertainty was rather large. A study done previously with the RPC OSLD system in photons

showed a drop of approximately 2% over the first 5 days post-irradiation (Homnick 2008).

Fading studies can show different results with different dosimetry systems due to the

reader and filters used as well as OSLD batch heterogeneities, so calibration of each system and

batch is recommended. It is worthwhile to investigate OSLD post-irradiation fading separately in

protons since the microscopic dose distribution is different than photons and influences the F^+-

center/UV proportion of emissions. To date, no explicit fading study of Al_2O_3:C in protons has

been done, although Yukihara & McKeever (2006a) have shown using low-LET irradiation that

the UV luminescence portion of total signal increases with time post-irradiation.

2.3.6   Angular Dependence

Angular dependence, a.k.a. directional dependence, has been briefly studied before in

literature. This study attempts to further characterize the angular dependence of OSLDs;

specifically for the new generation OSLD nanoDot. Because the line of OSLDs from Landauer

consists of thin disks of material encased in plastic with a small air gap, the irregular geometry

mandates that angular dependence is an important characteristic to determine. Angular

dependence of a given detector can be described by a function related to a reference situation:

$$k_{ang}(\theta) = h(\theta) * k_{ang}(\theta_0)$$

Equation 2.8 Angular dependence function.

where k_{ang} is the angular dependence factor of the detector, h is the directional dependence function, and θ_0 refers to a reference condition. This study aimed to determine h of the nanoDot in photons and protons relative to a reference condition.

At present, three studies have attempted to describe angular response of OSLDs, two in 6 MV photons and the other using various radioactive sources. The first study done by Aznar *et al.* (2004) used a small Al_2O_3:C crystal in an optical fiber setup for real-time OSL dosimetry. The crystal was put in a spherical phantom of 3 cm diameter filled with water. The study seemed to show no significant deviation in response with angle, but explicit uncertainty values were not stated. Since the crystal dimensions and casing were much different than that used in the current study the results from Aznar *et al.* 2004 should not strongly predict the dependence for this current study.

The second study was done by Mancosu *et al.* (2005) which looked at the TL response of both thin (≈40 μm) and relatively thick (1 mm) Al_2O_3:C dosimeters in response to both narrow and wide spot sources. A specially made irradiator was constructed to hold the dosimeter stationary while the source was rotated equidistantly around the dosimeter. Angular response depended on both the source and dosimeter type (thin or thick) but generally displayed a drop in signal relative to 0 degrees starting between 10 and 60 degrees from perpendicular, and with an end result of all the sample responses at 90 degrees (i.e. the plane of the dosimeter in line with the radiation field) dropping to less than 5% of the signal relative to 0 degrees. There are a number of causes for a certain level of signal reduction including beam attenuation and mean path lengths of the various energy sources. The signal of the highest energy beta source, ^{90}Y, displayed smaller angular dependence than the signal of the lower energy ones, which could indicate that angular dependence may carry an energy dependent effect, if for no other cases than radioactive sources.

In the third study, Jursinic (2007) irradiated the previous generation of Landauer dosimeters, the InLight dosimeter, in a 3.7 cm diameter water-equivalent cylindrical phantom (discussed further in Section 2.6.3) in 10 degree increments. No apparent dependence was found within an experimental uncertainty of ±0.9%. This study aimed at confirming the angular response of the new generation nanoDot in photons and defining response in protons.

2.4   Signal Readout Depletion

Being able to reread a dosimeter is an invaluable advantage. This allows another reading in the case of an unstable reading session, multiple readings for better statistics, and a permanent record that can be read again much later on if need be. However, each reading depletes the amount of trapped charge by a small fraction. For a comprehensive approach to partial-stimulation dosimetry this must be accounted for. Previous work shows that for the high-intensity stimulation used by the MicroStar the luminescence signal is reduced by approximately 0.2% per reading (Jursinic 2007). RPC protocol reads the OSLD three times consecutively. For a small number of readings like this the depletion correction is small, but is important to track if the dosimeter must be read out again.

Several times throughout this study, at the end of a OSLD reading session, one of the OSLDs read previously in the session was again read 20-25 times consecutively to determine the amount of signal depletion per reading. Approximately 6 dosimeters throughout the study were used to study signal depletion. Results showed an average drop of 0.15% depletion per reading. This is in agreement with previous work at the RPC (Homnick 2008).

2.5   Dosimeter Bleaching

OSL signal can be removed to reset the dosimeter for reuse. A reset can be accomplished by heating the dosimeter, annealing, or exposing it to light, bleaching. Removing all filled traps, including the DET requires annealing at a temperature of 900° C for 15-30 minutes (Akselrod *et al.* 1993). Because Landauer commercial dosimeters come inside a plastic casing for protection from unintentional light exposure, annealing cannot be utilized. Bleaching can be accomplished in almost any light, but the time required to remove trapped charge depends on the wavelength and intensity. Jursinic (2007) showed that with a 150 W Tungsten-halogen light source the signal could be reduced to less than 2% of the original signal after less than 1 minute of exposure, but took approximately 2 hours in bright room light to achieve >90% level of reduction.

At the RPC, OSLDs are bleached in a custom-built wooden cabinet, shown in Figure 2.6. The OSLDs sit on a clear plastic platform midway between the top and bottom of the cabinet. At the top and bottom are two 54-watt fluorescent bulbs with a step-filter around them. The filter is used to remove UV photons that could induce ionizations while bleaching. OSLDs are placed with the aluminum oxide disk unsheathed on the platform and exposed to the light source for 24 hours. Signal after bleaching is usually less than 0.3% of the original signal at 1 Gy.

Figure 2.6 OSLD bleaching box at the RPC.

2.6   Phantoms

2.6.1   OSL/TL Phantom

To compare TLDs and OSLDs a solid water phantom was used that allowed simultaneous irradiation of both types of dosimeters. The phantom used had been constructed previously for a similar RPC student project and is pictured in Figure 2.7. The solid water phantom measures 20x20x0.5 cm^3 and had a portion of the center milled out to allow dosimeters to be placed flush with the top surface. The total milled surface area is approximately 8 cm^2, which allowed a total of eight dosimeters to be placed within for each irradiation. This phantom was used for all irradiations comparing TLDs and OSLDs.

Figure 2.7 Solid Water phantom.

2.6.2   RPC Pelvic Phantom

The RPC has developed a number of anthropomorphic phantoms to be used in their mailable dosimetry protocol. One of these, a pelvic phantom for prostate treatment QA, was used in this study and has been shown to yield reproducible results with TLD measurements (Followill

et al. 2007). The phantom, pictured in Figure 2.8, is a hollow plastic case with a center removable insert made of high-impact polystyrene (HIPS). The HIPS is a near-water equivalent material, creating similar irradiation and scatter conditions to water. The outer shell of the phantom can be filled and drained with water for irradiation and storage respectively.

The phantom is designed to lock the insert at one angle for RPC phantom irradiation protocol. However, the insert was modified slightly to allow rotation to any desired angle. This rotation allowed the study of angular dependence. A diagram showing the OSLD inserts is shown in Figure 2.10. Two similar triangular inserts were manufactured to hold OSLDs in the dosimeter positions, one of which is shown in Figure 2.9. The center of each OSLD is located approximately 8 mm away from the axis of rotation of the HIPS insert (see Figure 2.10). It is important that this positioning is accounted for in the dosimetry and is discussed in Section 2.8.

Figure 2.8 Pelvic phantom front view.
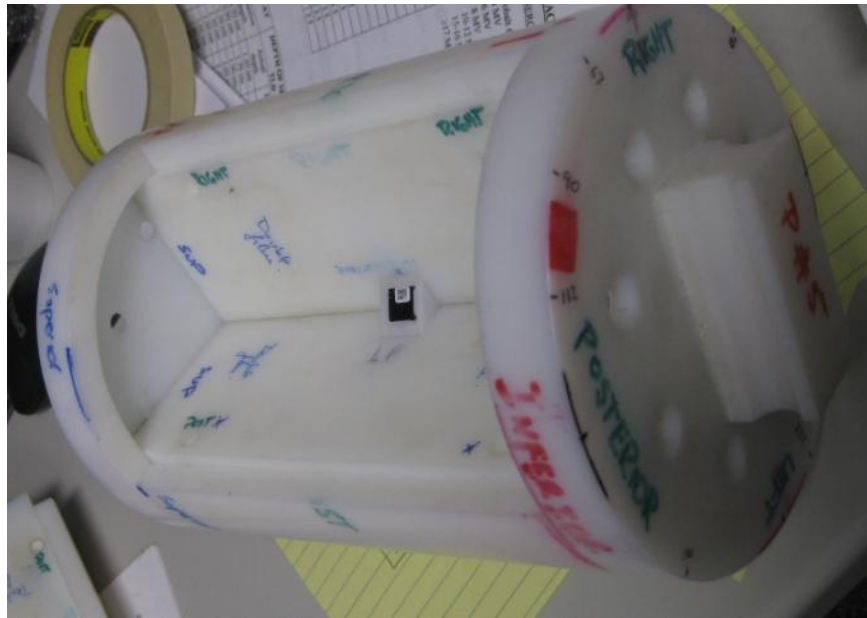
Figure 2.9 HIPS dosimetry insert with section removed showing one OSLD.
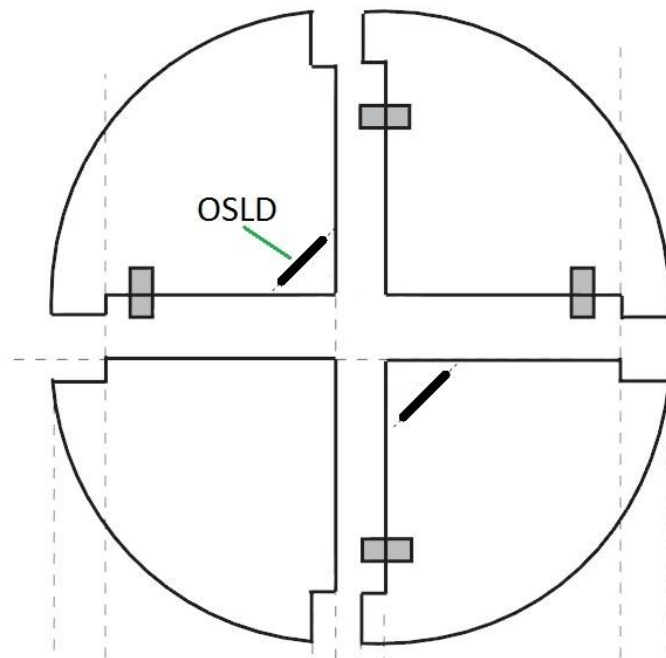
Figure 2.10 HIPS insert diagram showing OSLD positions.

2.6.3   Small Cylinder Phantom

After finding results that disagreed with previous work (discussed in Section 3.2) and after personal communication with Landauer, the author and Dr. Paul Jursinic from West Michigan Cancer Center traded phantoms. Dr. Jursinic's phantom was the same one used to find the results of his 2007 paper. The set up conditions of his phantom were described in the previously mentioned paper and were imitated as closely as possible for the respective experiment performed in this study.

Dr. Jursinic's phantom is a water-equivalent cylinder 5 cm in height and 3.7 cm in diameter and is shown in Figure 2.11. The cylinder is halved along the long axis to allow a dosimeter to be placed between the halves. A thin piece of "superflab", a bolus water-equivalent material, is laid between the halves with a cutout to specifically fit the nanoDot. A high-density Styrofoam block was designed to be used in conjunction with the phantom to mark degree values and to minimize scatter effects of the treatment table. The phantom and block are pictured together in Figure 2.12.
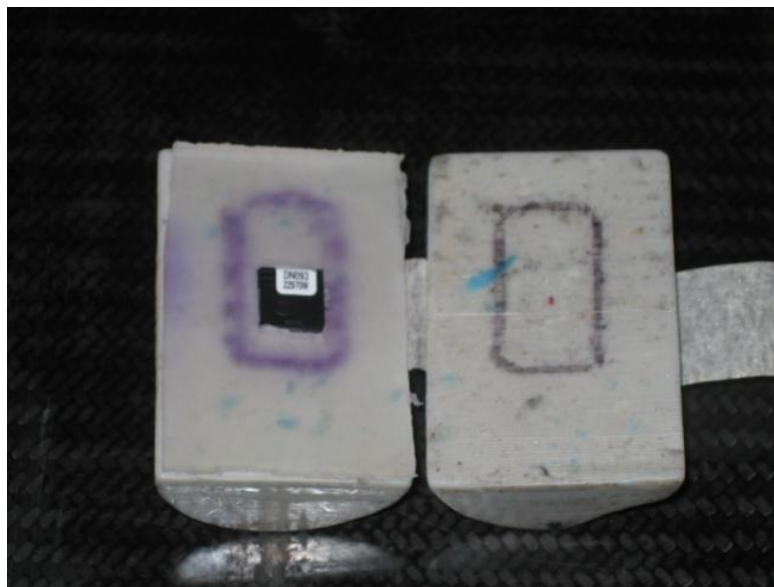
Figure 2.11 Small cylinder phantom open showing OSLD.
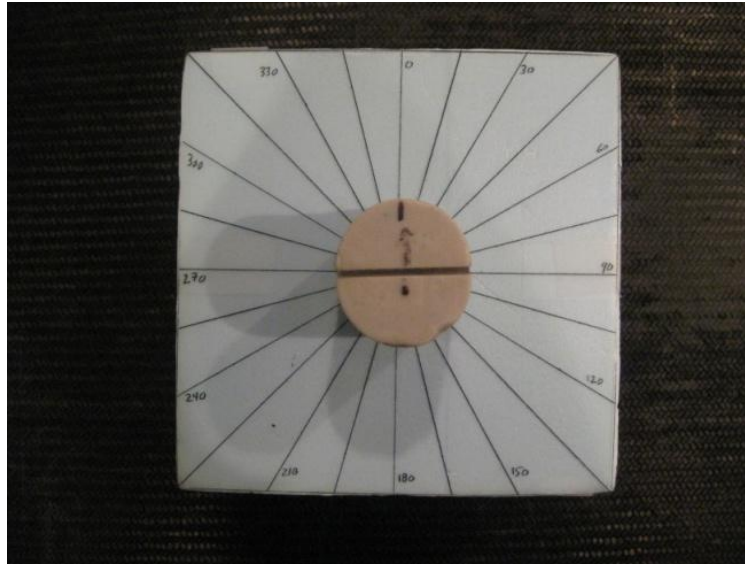
Figure 2.12 Cylinder phantom positioned on Styrofoam block.

2.7 OSL/TL Irradiations

2.7.1 OSL/TL Dosimeter Irradiation in cobalt-60

Cobalt irradiations were performed with a Theratron 780-C unit. The unit was recently

calibrated following the TG-51 protocol with an NEL ion chamber (IC) Model 2571 (Nuclear

Enterprises Ltd., Fairfield, NJ). The experimental setup for the dosimeter irradiation consisted of

the solid water phantom described in Section 2.6.1 and two $20x20x5$ cm^3 polystyrene blocks. One

block was placed below the phantom for backscatter and one above the phantom for buildup,

putting the dosimeters at 5 cm depth. The setup is similar to that for 6 MV photons, pictured in

Figure 2.13. The top of the upper block was placed at 80 cm SSD. Four TLDs and four OSLDs

were placed in the solid water phantom for each irradiation. Four irradiations of four dosimeters

of both TLDs and OSLDs were performed. For this study, flat plastic TLD packets were made to

fit the phantom which was created to accommodate OSLDs. The packets were hand-made, filled

with approximately 25 mg of RPC TLD-100 powder, and measured approximately $1x1x0.1$ cm^3.

The following general formula can be used to calculate the desired delivery system timer value, *Timer*, of exposure of the dosimeters to the cobalt source:

$$Timer = \frac{D}{Calib * DF * OAF * PDD * FS * Att}$$

Equation 2.9 Cobalt-60 timer calculation.

where *D* is the desired dose, *Calib* is the Gy/minute TG-51 calibration, *DF* is the decay factor of the cobalt, *OAF* is the off-axis factor, *PDD* is the percentage depth dose, *FS* is the field size factor, and *Att* is the attenuation factor for non-water mediums. Notice there is no inverse-square correction term. Since the experimental setup and TG-51 setup are both at 80 cm SSD, there is no need for a correction.

The decay factor corrects for the nuclear decay of the source of initial activity A_0 after *x* number of days from a reference time, given a cobalt-60 half-life of 1921.2 days (5.26y $*$ 365.25$\frac{d}{y}$), and is determined by following the generic exponential decay equation:

$$A = A_0 * e^{(-0.693 * \frac{x}{1921.2})}$$

Equation 2.10 Exponential cobalt-60 decay equation.

The attenuation factor describes the ratio of attenuation coefficients in media. Polystyrene was used in the OSL/TL photon experiments for buildup and must be related to water. This can be accomplished by using a scaling factor, comparing the linear attenuation coefficients of the mediums (Task Group 21 1983). To determine this scaling factor, the mass attenuation coefficients from NIST were used. The values were then multiplied by the density of their respective material, demonstrated in Equation 2.11. The values were nearly constant from cobalt-

47

60 to the MV range, so one ratio was used. So then, for the experiments using polystyrene as

buildup, an attention factor of 0.976 is used.

$$Att = \frac{\left(\frac{\mu}{\rho}\right)_{poly} * \rho_{poly}}{\left(\frac{\mu}{\rho}\right)_{water} * \rho_{water}} = \frac{u_{poly}}{u_{water}} = 0.976$$

Equation 2.11 Polystyrene attenuation scaling factor.

The *Timer* value refers to the ideal situation that the source is brought out and retracted

instantaneously. Because of the travel time of the source to the irradiation position, this must be

accounted for when calculating dose. The effective time of travel of the source is 0.011 minutes,

using equations from Orton & Siebert (1972), also called the end effect. Rearranging Equation

2.9, this can be expressed to include the end effect using the *Timer* value (expressed in minutes)

to find a calculation of *Total Dose*:

$$Total\ Dose = (Timer + 0.011) * Calib * DF * OAF * PDD * FS * Att$$

Equation 2.12 Cobalt-60 total dose calculation.

All the shared terms of Equation 2.9 and Equation 2.12 hold the same definition.

2.7.2 OSL/TL Dosimeter Irradiation in 6 MV Photons

All 6 MV photon irradiations were done on a Varian 21EX linac (Varian Medical

Systems, Palo Alto, CA). The linac was calibrated using TG-51 protocol. Prior to any irradiation,

a quality assurance check was performed for the 6 MV photon beam to ensure output was within

tolerance. This check used a PTW TN30010 ion chamber (PTW, Freiburg, Germany) calibrated

by an ADCL, laid within polystyrene blocks and was the same chamber used in the TG-51 calibration.

The setup for the 6 MV irradiation was similar to that for cobalt-60. The surface of the upper block of polystyrene was set to 100cm SSD and centered on the beam axis. The field size was set to 10x10 cm^2 with a gantry angle of 0° for the set up shown in Figure 2.13.
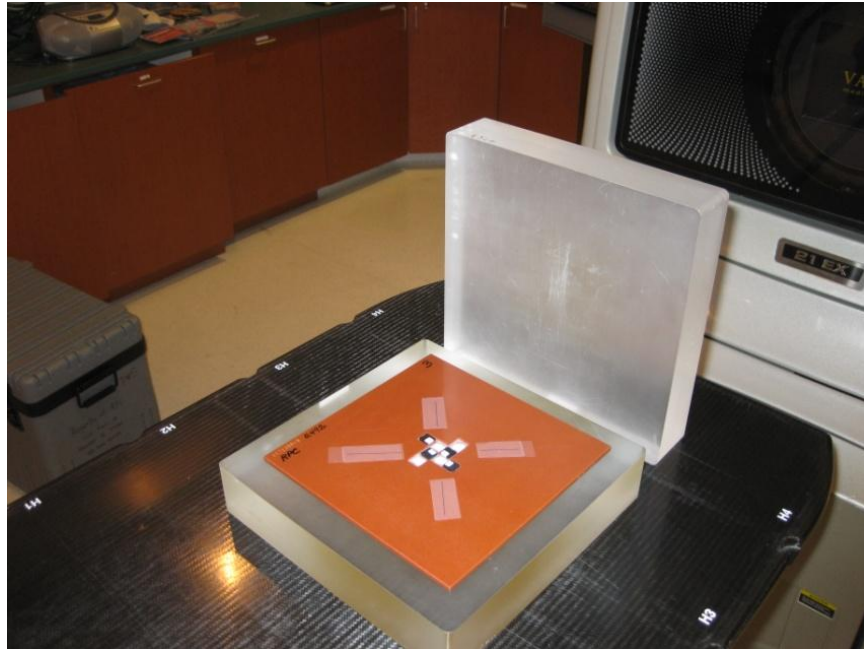
Figure 2.13 Solid Water phantom in position placed between two 5 cm polystyrene blocks (top block moved for visualization).

In general, dose can be calculated using a similar equation to Equation 2.12 but no decay factor or timer error correction is necessary:

$$D = MU * Calib * OAF * PDD * FS * Att$$

Equation 2.13 Linac dose calculation.

where *D* is absolute dose received, *MU* is the monitor unit setting of the linac, *Calib* is the cGy/MU TG-51 calibration and the other factors are the same as Equation 2.12.

2.7.3   OSL/TL Dosimeter Irradiation in 200MeV Protons

For the proton measurements, dosimeters were irradiated in the 200 MeV beam at the PTCH which was calibrated using the International Atomic Energy Agency (IAEA) Technical Report Series (TRS) 398 protocol (Andreo *et al.* 2000). The beam was used along with the large snout and a field size of 15x15 cm^2 at isocenter, with an SOBP of 10 cm. The setup is shown in Figure 2.14. This consisted of 14 cm of plastic water buildup, the solid water phantom, and a 5 cm water block for backscatter thus putting the dosimeters in the center of the SOBP.
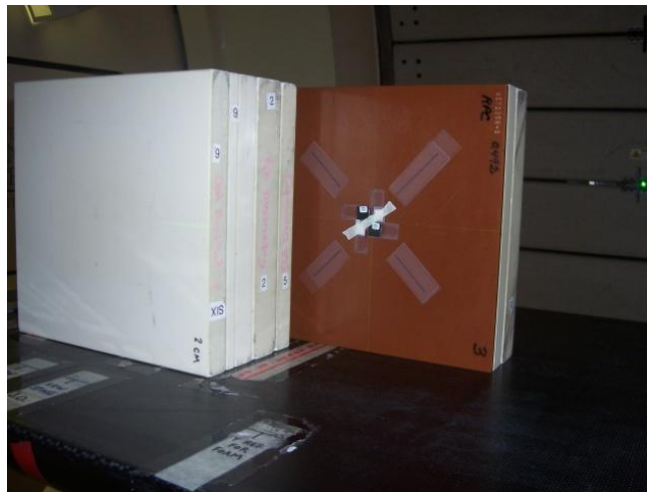
Figure 2.14 Solid Water phantom positioned for proton irradiation.

Figure 2.15 Side view of proton OSL/TL irradiation.

Output, and thus dose, for a given setup in protons can be determined with a number of correction factors. An equation to determine output, *d/MU*, has been proposed by Sahoo *et al.* (2008):

$$\frac{d}{MU} = ROF * SOBPF * RSF * SOBPOCF * OCR * FSF * ISF * CPSF$$

Equation 2.14 Proton output calculation using reference factors.

where the output *d/MU* is the measure of cGy/MU, ROF is the relative output factor, SOBPF is the SOBP factor, RSF is the range shift factor, SOBPOCF is the SOBP off-center factor, OCR is the off-center ratio, ISF is the inverse-square factor, FSF is the field size factor, and CPSF is the compensator and patient scatter factor. Most factors are referenced to measurements in water with a parallel plate ion chamber in the PTCH's 250 MeV beam using the medium snout with 10x10 cm^2 field size and SOBP of 10 cm and all factors are listed in the above mentioned work. From here, the MU setting to use to deliver dose *D* is calculated simply as:

$$MU = \frac{D}{\frac{d}{MU}}$$

Equation 2.15 Proton dose calculation.

Using Equation 2.15 to calculate output is considered accurate, but was used as a secondary check of delivered dose. Because of the general complexity of the proton delivery system, parallel plate ion chamber readings with a PTW Markus Model 23343 (PTW, Freiburg, Germany) were taken at the dosimeter depth with the set up described above prior to irradiation. The readings were converted to determine a specific output following the formula:

$$\frac{cGy}{MU} = \frac{Rdg * C_{tp} * N_{D,w} * K_q * K_s * K_{pol}}{MU}$$

Equation 2.16 Proton output calculation using an ion chamber.

where the left side of the equation is the output, Rdg is the ion chamber reading for the specific setup, C_{tp} is the temperature & pressure correction, $N_{D,w}$ is the IC calibration of dose to charge, K_q is the beam quality factor of the IC, K_s is the ion recombination correction of the IC, and K_{pol} is the polarity correction factor of the IC. This output was compared to that determined by Equation 2.14 to ensure stability of the proton delivery system. From here, desired dose and the output were put into Equation 2.15 to determine the correct MU value.

2.8   Angular Dependence Irradiations

2.8.1   Pelvic Phantom Angular Dependence

To study angular dependence the pelvic phantom was set up with a fixed gantry angle of 0 degrees, directly above the phantom, shown in Figure 2.16. This setup was stationary except for

the cylindrical insert, allowing consistency in linac output and depth dose. The cylindrical insert was rotated through a total of 12 angles. For each angle, between 2 and 3 irradiations of 2 OSLDs each were performed. The dosimeters were placed in the phantom such that both were facing the same direction. Thus, all dosimeters irradiated at a given angle were facing the same way.
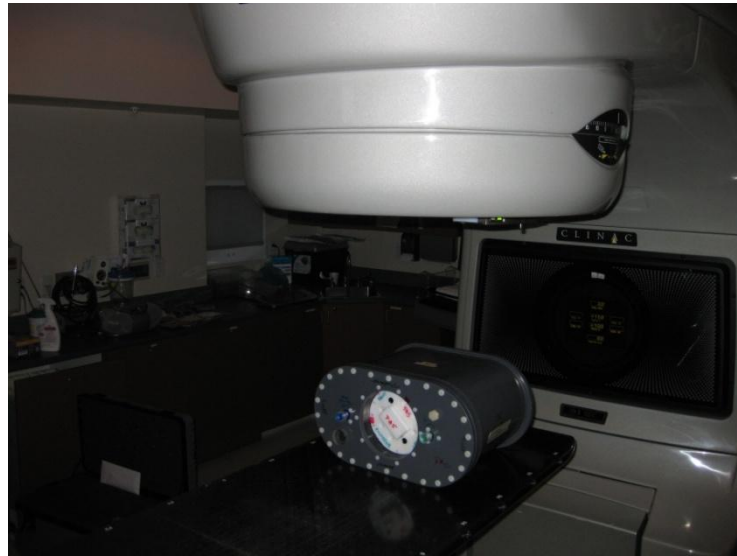
Figure 2.16 6 MV photon angular dependence setup using the pelvic phantom.

The center of the cylindrical insert was set to isocenter, putting each dosimeter approximately 8 mm from isocenter at any given angle, shown in Figure 2.17.

Because of the dosimeter displacement from the cylinder center, and thus the dose calculation point, the dose received by each dosimeter for a given angle differed. However, because the displacement was symmetric on either side, the average of the dosimeter response was used as the given dose to the center. For each irradiation, the insert had to be removed, exposed OSLDs removed and new ones put in. Angle marks on the insert allowed it to be placed at the same angle consistently.

2.8.1.1 Photons

The photon irradiations were performed in a 10x10 cm^2 field at 6 MV. While a hand calculation could be done to determine the necessary MU's to deliver the desired dose, the phantom was simulated in an AcQsim CT scanner (Philips Medical Systems, Andover, MA) and brought into the Pinnacle treatment planning system (TPS). One beam was used in the plan, set to irradiate from 0 degrees and to deliver 100 cGy to isocenter. The pelvic phantom was set to 90 cm SSD, putting the center of the cylindrical insert very near to isocenter.
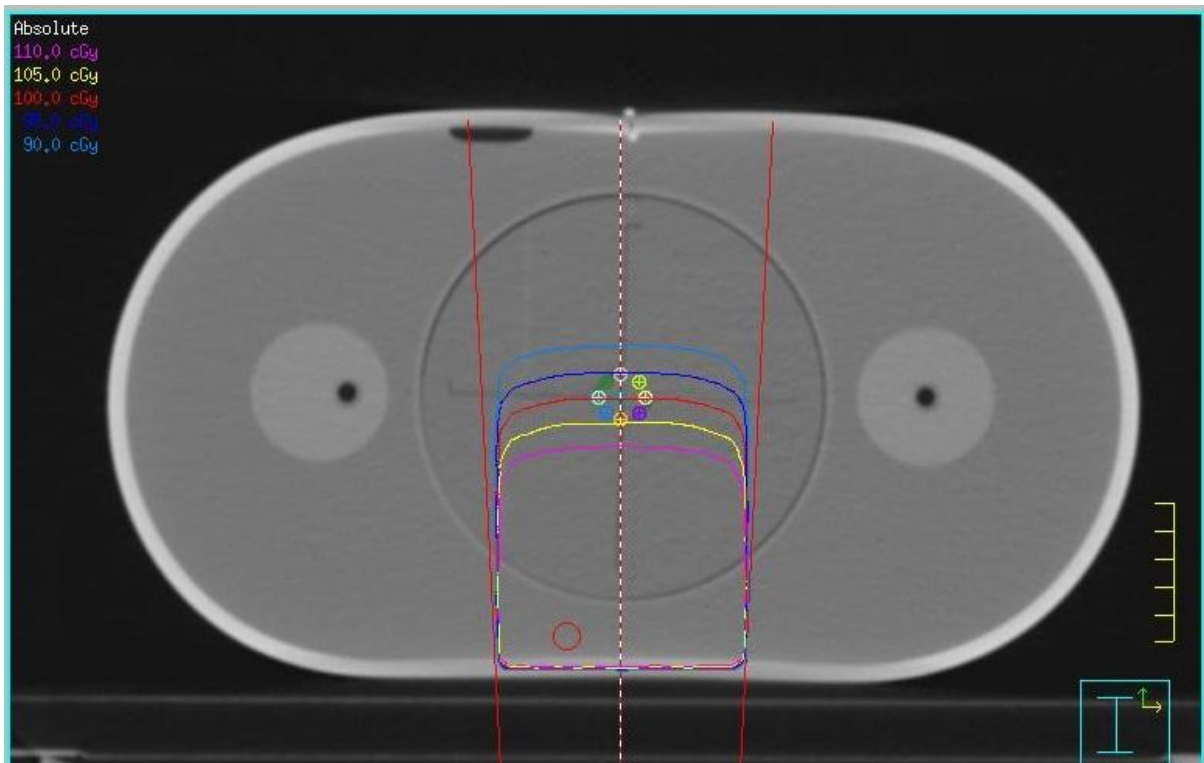
Figure 2.17 CT screenshot of the treatment plan of the pelvic phantom. While the beam is shown coming from 180 degrees, the phantom was laid posterior-anterior (simulated and thus here shown in anterior-posterior) for the irradiation. The blue, red, and yellow isodose lines represent 105, 100, and 95 cGy respectively.

2.8.1.2 Protons

Irradiations in protons followed a similar set up as described for photons. A 200 MeV
beam (19 cm range) was selected, the gantry set to 0 degrees, and 15x15 cm^2 field size used along
with a 10 cm SOBP. The center of the cylinder was set to isocenter, and 4 cm of plastic water was
used for buildup on top of the phantom, shown in Figure 2.18, to place the dosimeters in the
middle of the SOBP.
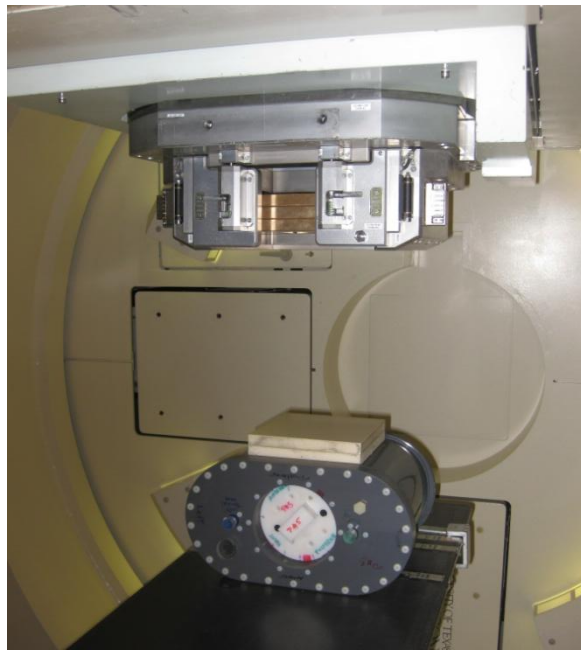
Figure 2.18 Proton angular dependence setup using the pelvic phantom.

2.8.2 Small Cylinder Phantom Angular Dependence

For irradiation of the small cylindrical phantom, the linac gantry was turned to 270
degrees then plumbed with a level. The phantom and block were set up on the treatment table
such that the center of the cylinder, and thus the dosimeter, was at isocenter, shown in Figure

2.19. A 10x10 cm^2 field size was used, as in Jursinic (2007). As with the pelvic phantom, 0

degrees corresponds to the dosimeter front being normal to the radiation beam. To study angular

dependence the cylinder was rotated about the vertical axis. One dosimeter was irradiated at a

time, and three irradiations were done at each angle, all at 6 MV.
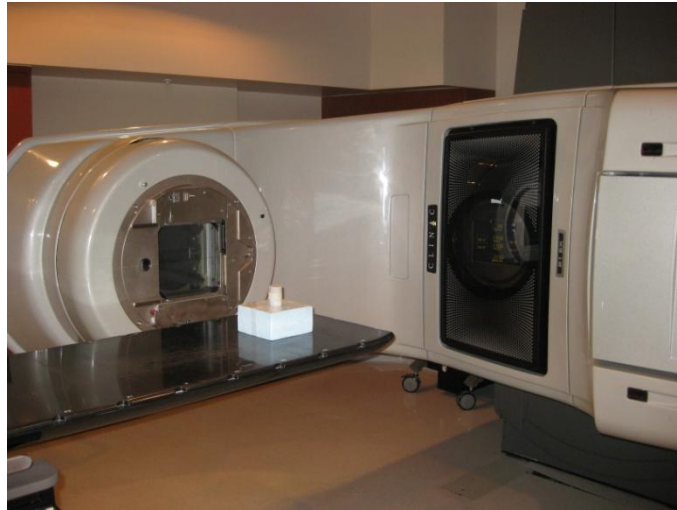
Figure 2.19 Photon angular dependence setup using the small cylinder.

2.8.3   Pelvic Insert Angular Dependence

An experiment was also run using just the pelvic phantom HIPS dosimetric insert. This

experiment was performed in response to the results of the pelvic phantom and small cylinder

phantom (discussed in Section 3.2.1.1 & 3.2.2). This setup was used by Dr. Jursinic during the

phantom swap as well, and is shown in Figure 2.20. The gantry was turned to 90 degrees and set

to a 10x10 cm^2 field. The insert was set such that the center of the insert was at isocenter. Marks

on the insert aligned with the room lasers allowed for consistent placement at all angles. Four

angles were used, with 3 irradiations at each angle. Both 6 MV and 18 MV experiments were done using this set up.
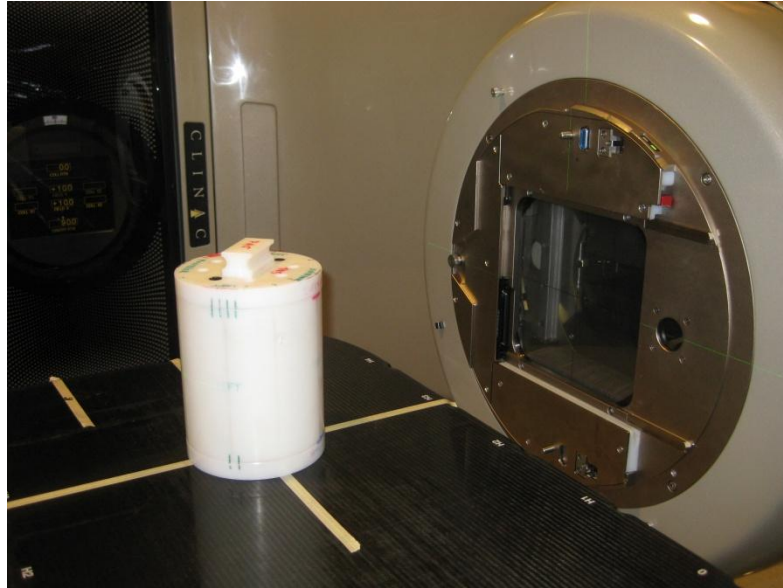
Figure 2.20 Pelvic phantom HIPS angular dependence setup.

2.9 Fading

A study of post-irradiation signal fading was performed for Al_2O_3:C in response to protons. Since the RPC protocol reads OSLDs days to weeks after irradiation, the fading on the order of days was studied. To date, no explicit study of fading in protons has been done for this dosimetry system. Because of the dose distribution in HCPs, with proportionally more DETs getting filled, Al_2O_3:C may not exhibit fading to the same extent as photons.

Six irradiations were performed at specific times and read out in one session to reduce system sensitivity uncertainty. The irradiation setup was the same in every instance. The beam was set to 160 MeV (13 cm range), 10x10 cm^2 field size and a SOBP of 6 cm. Set up appeared similar to that of the 200 and 250 MeV OSL/TL irradiations, pictured in Figure 2.15. A total of 10 cm of plastic water was used for buildup with the solid water OSL/TL phantom behind it,

putting it at the center of the SOBP. An additional 4cm of plastic water was used behind the phantom for backscatter. Six OSLDs were irradiated for each time point. The irradiations were spaced out between 1 month and 1 day prior to reading. Output of the beam at the dosimeter depth was determined before each irradiation, just as for the OSL/TL irradiations, with a parallel-plate ion chamber.

2.10 Proton Energy Dependence

A measurement of OSL RLE was done for select proton energies. The OSL/TL experiment used the 200 MeV beam, and the fading study used the 160 MeV. A separate OSLD-only irradiation was performed using the 250 MeV (28.5 cm range) beam. This is the beam that most other proton energies are referenced to when using Equation 2.14. The 250 MeV beam was not used for the OSL/TL experiment as there were technical difficulties with the delivery system at the time of the experiment. The setup for the 250 MeV was similar to the others. A 10x10 cm^2 field was used along with a 10 cm SOBP. A total of 23.5 cm of plastic water was used for buildup in front of the solid water phantom with 8 cm behind it. An output value was determined with an IC at the dosimeter location before irradiation.

Since the irradiations were done in the SOBP, the differences energy spectra at the dosimeter locations were relatively large. Within the SOBP, there are protons expending the last of their energy as well as protons that have the residual energy remaining to reach the end of the SOBP. Since the spectrum of energies at a specific point within an SOBP is somewhat similar despite the nominal energy, the response should theoretically also be relatively similar.

58

Chapter 3 – Results & Discussion

3.1 OSL/TL Irradiation

3.1.1 Cobalt-60 Irradiation

Irradiations in cobalt-60 were carried out according to the setup described in Section 2.7.1. Four consecutive irradiations were performed with the same set up. For convenience the unit timer was set to expose the dosimeters for 2.00 minutes each time and dose was calculated using Equation 2.12. The calculated dose received by the dosimeters is thus:

$$Dose\ (cGy) = (2.00 + 0.011) * 35.11 * 0.9786 * 1 * 1 * 1 * 0.976 = 68.11\ cGy\ (muscle)$$

Equation 3.1 Cobalt-60 dose determination.

The OSLDs were read 5-10 days after irradiation and TLDs at least two weeks. Dose received by the OSLDs was calculated using Equation 2.7 and dose for TLDs with Equation 2.2. The standards used to determine the sensitivity factor were irradiated in the same week as the experiment.
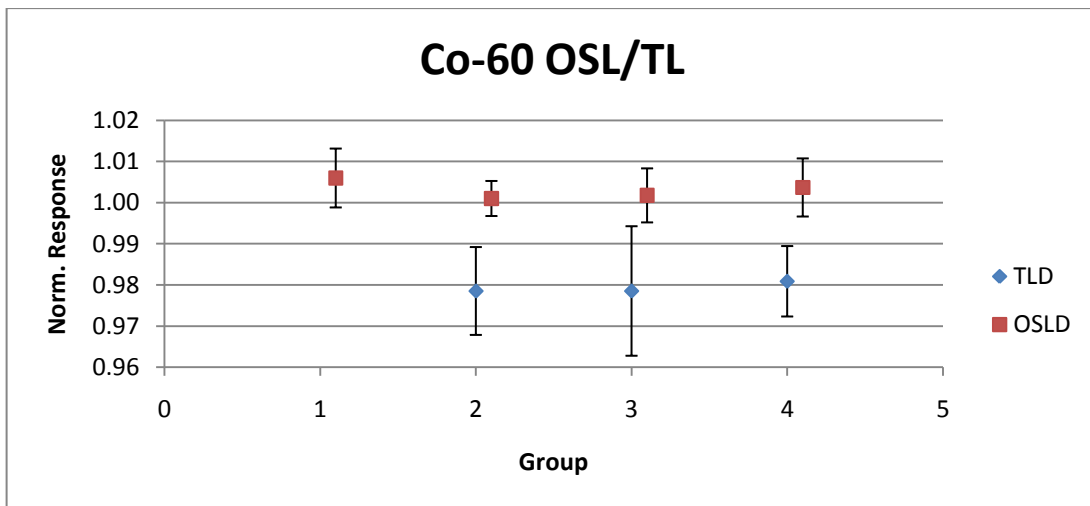
Figure 3.1 Cobalt-60 OSL/TL comparison. Error bars will always represent 1 standard deviation of the experimental mean.

From the results shown in Figure 3.1, it can be seen that the doses determined from the cobalt-60 irradiation for OSLDs were within 1% of the calculated dose. Since the standards that convert counts to dose were also irradiated in a cobalt-60 beam, agreement with calculation is expected. Experiments were performed with a different cobalt-60 unit than was used to irradiate the standards.

The TLD results were less precise and less accurate compared to the OSLDs, apparently having a systematic error. The results of the first group of TLDs was >5% from the calculated dose with a large standard deviation, so it was removed from the results. Because the raw TL readings showed large standard deviations in some cases, the results proved to have relatively large uncertainty. Since both the OSL and TL dosimeters of each group received the same dose, the under response of the TLDs would indicate some kind of misreading or mishandling of the dosimeters. This would be a cause for concern, but the RPC has been using a dependable reading protocol for a very long time with consistent and accurate results, thus pointing to a systematic error of this specific irradiation experiment. Even so, a second experiment was performed with the same set up, and with similar results to Figure 3.1, again pointing to a systematic reading or handling error.

The biggest difference between the standard RPC TLD capsule normally used and this set of experiments was the encapsulation of the TLD power. Hand-made flat packets were constructed by the author, made to fit the special solid water phantom. Instead of being the normal cylindrical shape, the powder was flattened in square plastic sheets and sealed. The powder used was taken directly from RPC TLD capsules. The amount of powder in the packets was slightly more than the amount in a normal RPC capsule.

3.1.2   6 MV Irradiation

Irradiation conditions at 6 MV were similar to that of cobalt-60. Four irradiations of four OSLDs and TLDs each were performed. OSLD results were converted to absolute dose and compared to the Equation 2.13 TG-51 calculated dose. The calculated dose received by the dosimeters was:

$$D = 116 * 0.999 * 1 * 0.861 * 1 * 0.976 = 97.38 \text{ cGy } (muscle)$$

Equation 3.2 Linac dose determination.

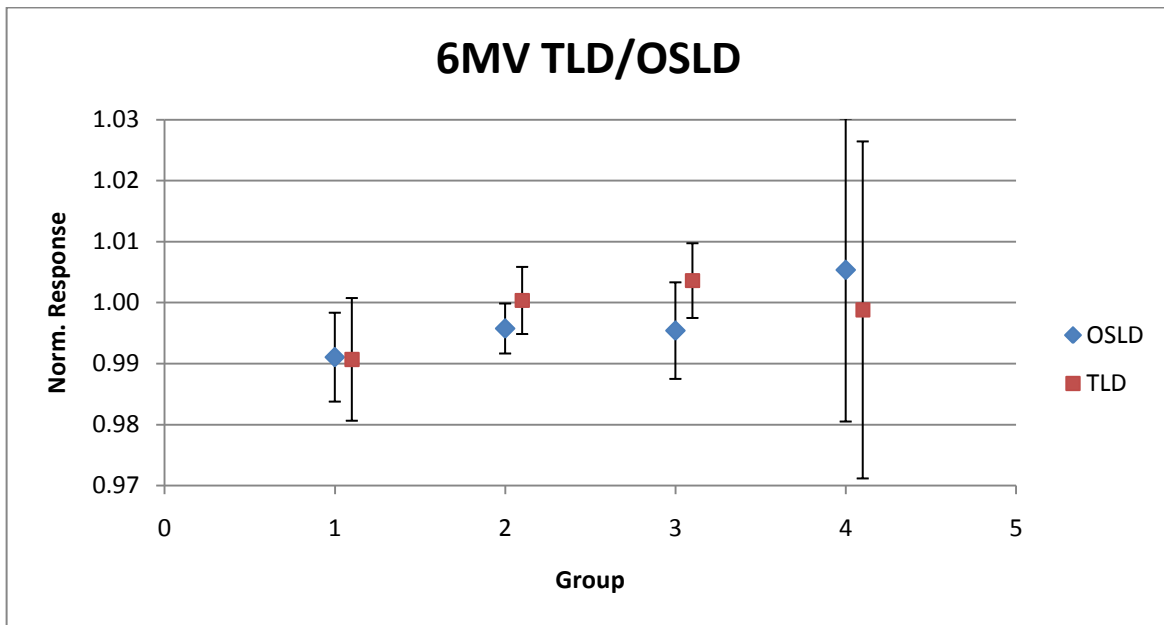OSLDs were again read 5-10 days after irradiation and TLDs at least two weeks.

Figure 3.2 6 MV OSL/TL comparison.

Figure 3.2 shows that with the exception of the uncertainty of the Group 4 irradiation, the dose response results of the 6 MV irradiation were similar. The average of the data for each type of dosimeter was less than 1% different than the TG-51 calculated dose. OSLD data had an

average response of 0.997 relative to the TG-51 calculated dose, and TLD data had 0.998. Again, the OSLD and TLD absolute dose was determined with Equation 2.7 and Equation 2.2 respectively. Since the absolute dose of the dosimeters was determined by the sensitivity to cobalt-60, it is clear that there is little energy dependence of the dosimeters between cobalt-60 and 6 MV photons. Viamonte *et al.* (2008) showed no energy dependence of Al_2O_3:C for megavoltage beams, but an over response for cobalt-60 of approximately 4% relative to the MV beams. The reason for the over-response and difference from this study is unclear. Previous work both in literature and at the RPC showed sensitivity at 6 MV to be equivalent to cobalt-60 within experimental uncertainty (Yukihara *et al.* 2008; Homnick, 2008).

3.1.3   Proton Irradiation

Proton irradiations consisted of four irradiations of four TLDs and OSLDs, just as done in photons. The proton beam nominal energy was 200 MeV (19 cm range) and a SOBP of 10 cm was used. Before the dosimeter irradiation, 50 MUs were delivered to the parallel plate ion chamber and the output factor was determined to be:

$$Output = \frac{0.8104 * 1.008 * 55.91 * 1.002 * 1.002 * 1}{50} = 0.915 \frac{cGy}{MU} \ (water)$$

Equation 3.3 Ion chamber-determined proton output factor.

This was the output used to determine the desired experimental MU setting. It can be compared to the stated output calculated from Equation 2.14 using the factor values found in Sahoo *et al.* (2008):

$$\frac{d}{MU} = 0.921 * 1 * 1 * 1 * 1 * 1.002 * 1 * 1 = 0.922 \frac{cGy}{MU} \ (water)$$

Equation 3.4 Reference-factor determined proton output.

The proton field size factor was small, increasing from 1 to 1.004 when going from

10x10 to 18x18 cm^2 field size, so the value used above (1.002) was interpolated. Since the

measured output was within 1% of the stated output, the measurement was considered within

tolerance and the measured output used for dose calculations. From here, the desired dose was

input into Equation 2.15 to determine the MU value:

$$MU = \frac{100 \ cGy}{0.915 \frac{cGy}{MU} \ (water)} = 109.3 \ MU$$

Equation 3.5 Proton dose determination.

The dosimeters were then irradiated to this MU value and results of the OSL/TL proton

irradiations are shown in Figure 3.3. The data for OSLDs are consistent, but systematically under

responded compared to the calculated and TLD doses. This under response agrees with previous

studies and predictions (Sawakuchi *et al.* 2008a; Sawakuchi *et al.* 2008b; Gaza *et al.* 2004; Gaza

et al. 2006; Edmund *et al.* 2007; Yukihara & McKeever 2006b; Yukihara *et al.* 2006) that shows

Al$_2$O$_3$:C response is reduced in HCP irradiation.
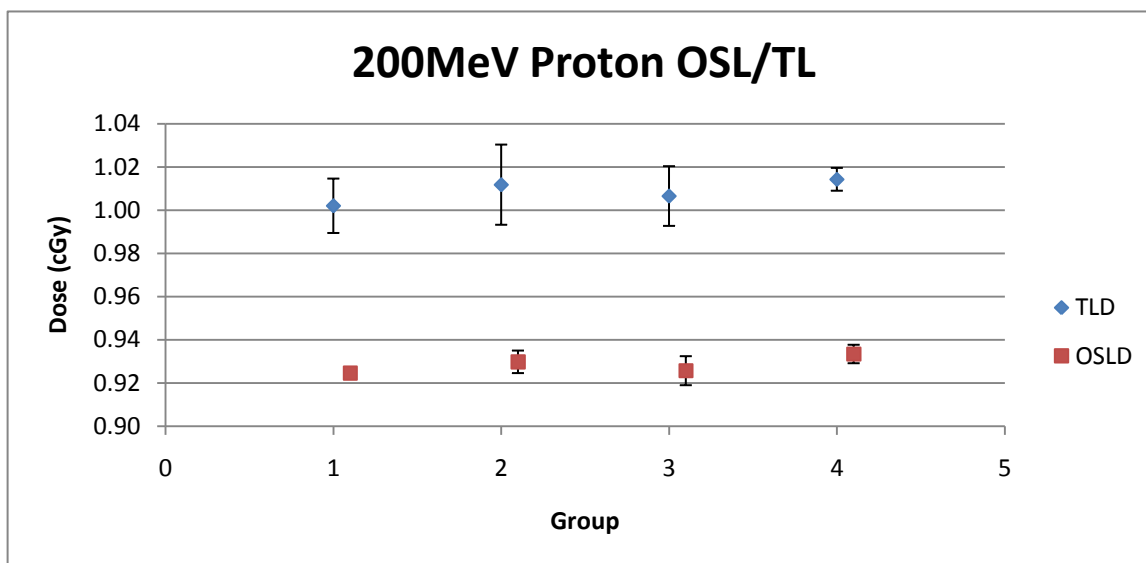
Figure 3.3 200 MeV proton OSL/TL comparison.

In this OSL/TL experiment, OSLD signal consistently responded 6-8% lower than calculation as shown in Figure 3.3, due largely to absorbed dose differences of aluminum oxide in cobalt-60 and protons. This and other reasons for under response are discussed further in Section 3.4.

TLDs had a consistent response, with an average dose approximately 1% higher than the calculated dose. No energy correction factor was used in the dose calculation since the RPC has so far not observed significantly difference energy response for TLD-100 in protons (Ibbott *et al.* 2008). However, the uncertainty in that data is large enough to accommodate the finding in this study. The calculated dose is considered reliable as an IC calibration was performed immediately preceding irradiation and also agreed within tolerances to commissioning output data as shown earlier.

It is important to note that absorbed dose is calculated to water at the PTCH, as per the IAEA TRS 398 protocol. The dosimeter standards irradiated in cobalt-60 are calculated to

muscle, thus we converted the dose results from one medium to the other. Note that this does not imply variation in absorbed dose, only that the calibration medium is different between protons and the reference beam, cobalt-60. Because of often unclear and ambiguous semantics regarding absorbed dose in protons for different mediums, the dose reported for protons for this study have all been related to water. So, the cobalt-60 reference dose was converted to dose to water. Absorbed dose to water in cobalt-60 can be determined from absorbed dose to muscle and mass energy-absorption ratios. According to AAPM TG-21 (1983):

$$D_{water} = D_{muscle} * \mu_{en}/\rho_{muscle}^{water}$$

Equation 3.6 Water-muscle dose conversion.

Mass energy-absorption ratios are found from the NIST data, just as for Al_2O_3:C absorbed dose calculation, to determine the equivalent dose to water. The resulting dose to water for standards referenced in muscle is:

$$D_{water} = 100\ cGy\ (muscle) * \left(\frac{1}{0.99}\right) = 101\ cGy\ (water)$$

Equation 3.7 Cobalt-60 dose to water from muscle.

Equation 3.7 says that relative to our cobalt-60 standards which received 100 cGy in muscle, the dosimeters received a dose of 101 cGy in water. The dosimeters in protons can then be directly compared to the cobalt standards. For this study, this comparison is not equated with the cobalt Gray equivalent (CGE) term, which describes dose in protons in terms of an equivalent dose in cobalt-60, but in reference to patient equivalent dose, not necessarily absorbed dose. At this point, after examining the data, a correction factor can be posited for OSLDs in proton beams, discussed in Section 3.4.

3.2 Angular Dependence Irradiation

3.2.1 Pelvic Phantom Angular Dependence Irradiation

3.2.1.1 Photon Irradiation

Photon angular dependence data were collected in several sessions with the same linear accelerator. The first session irradiated 6 OSLDs every 45 degrees from 0 – 315 degrees. Upon initial analysis a possible dependence was seen at angles perpendicular to the beam as shown in Figure 3.4. A second set of data was collected at intermediate angles on both sides of 90 and 270 degrees, shown in Figure 3.5. Thus, the second irradiation collected OSLD data at 0 degrees for re-reference, and angles 67 and 112 (90 ± 22), 247 and 292 (270 ± 22) degrees. This data set was normalized to the 0 degree data of that session and then aggregated with the first data set for a cumulative set shown in Figure 3.6. The results shown on that figure demonstrate a smooth response of OSLD signal as a function of angle with a drop in signal at the 90 & 270 degree points. While the reference response (0 degrees) has a relatively large uncertainty, the average uncertainty at the other angles show a tight distribution, usually less than $\pm 0.4\%$. Thus, the angular dependence noticed at the extreme angles cannot simply be ignored due to experimental uncertainty.
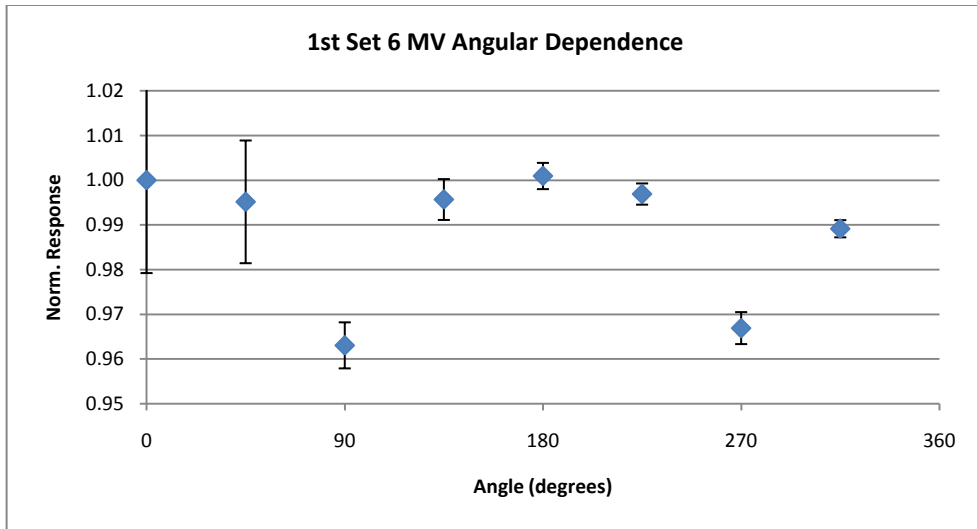
Figure 3.4 First 6 MV angular dependence data set.
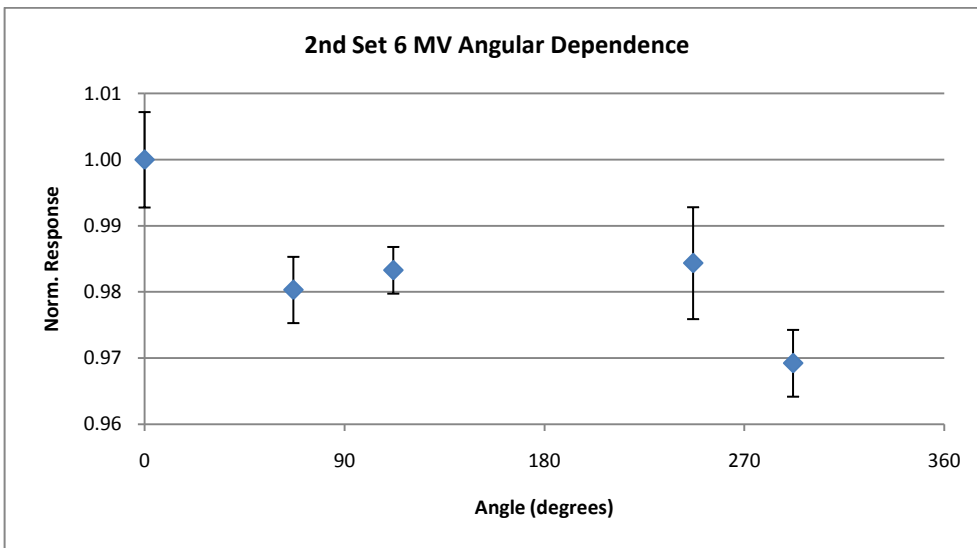
Figure 3.5 Second 6 MV angular dependence data set.
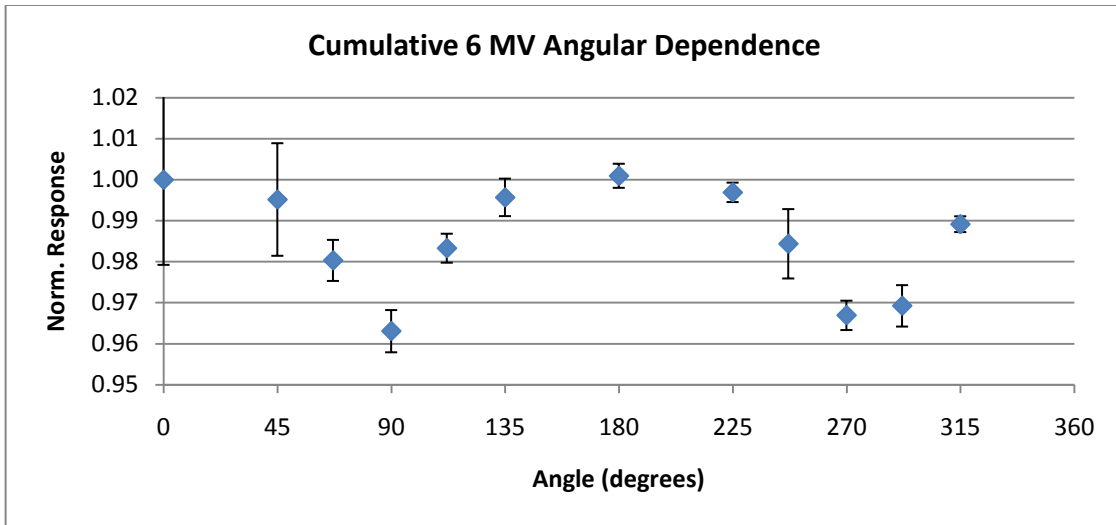
Figure 3.6 Cumulative 6 MV angular dependence data.
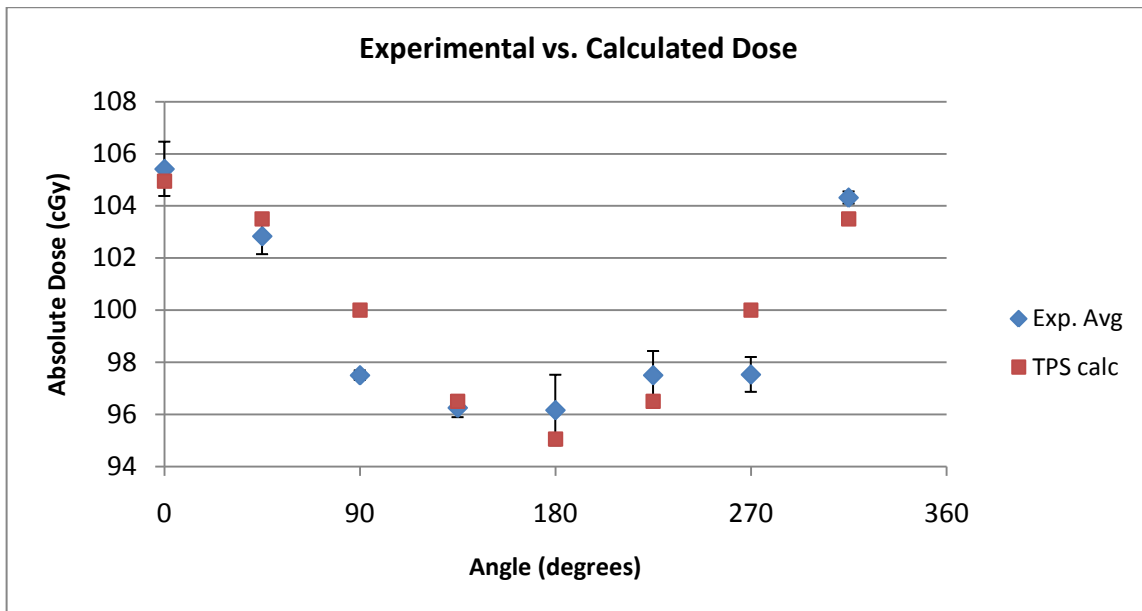
Figure 3.7 Experimental 6 MV angular dependence data compared with TPS calculated

doses.
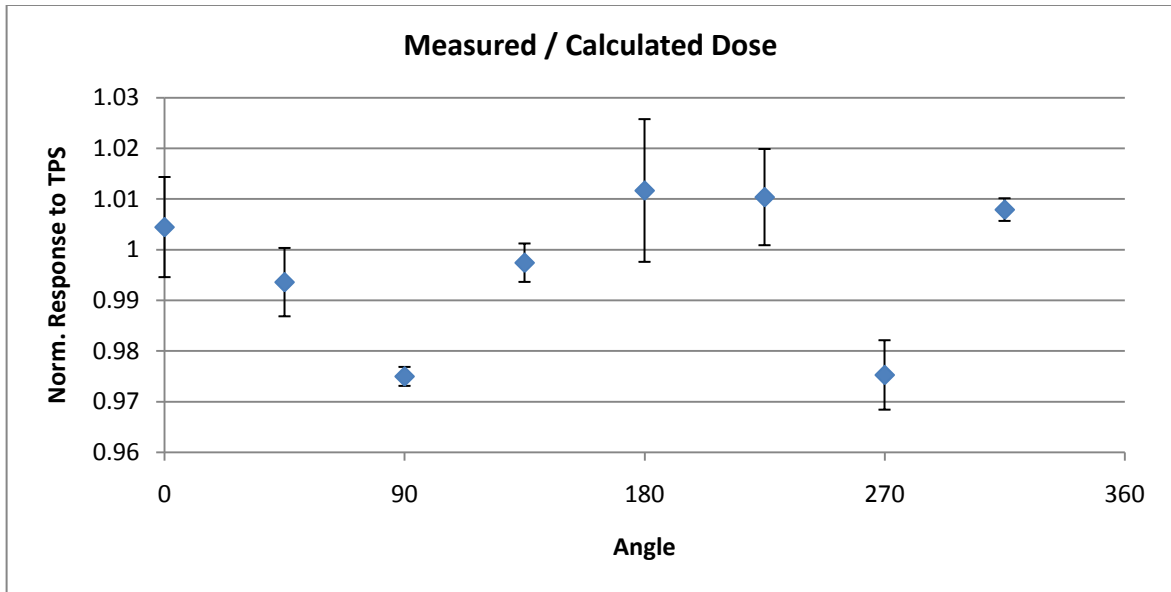
Figure 3.8 6 MV angular dependence data normalized to the TPS calculated dose.

The relative response of the nanoDot dosimeters was found to be approximately 4% lower at angles where the dosimeter is parallel with the radiation field compared to perpendicular. The results were then compared to the TPS calculated doses at the points shown in Figure 2.17 and are shown in Figure 3.7 and Figure 3.8. The results of the OSLD to TPS comparison also showed an under response of the dosimeter at angles approaching 90 & 270. The results shown in Figure 3.6 are then in agreement with those shown in Figure 3.8

After these two sets were analyzed, one more set was taken to confirm previous results. Data were taken only at the primary angles (0, 90, 180, & 270 degrees) and is shown in Figure 3.9. TLDs were also irradiated immediately following the third OSLD irradiation to determine if possible heterogeneities in the pelvic phantom might have had an effect on the dosimeters. Triangular inserts similar to the ones used for OSLDs were used, specifically holding TLD capsules approximately 5 mm off-center. A demonstration of angular dependence for TLDs would indicate heterogeneity in the phantom and invalidate the angular dependence results for

OSLDs. Data from the TLD irradiations are shown in Figure 3.10. The TLDs showed a similar response at all angles, indicating no angular dependence within experimental uncertainty.
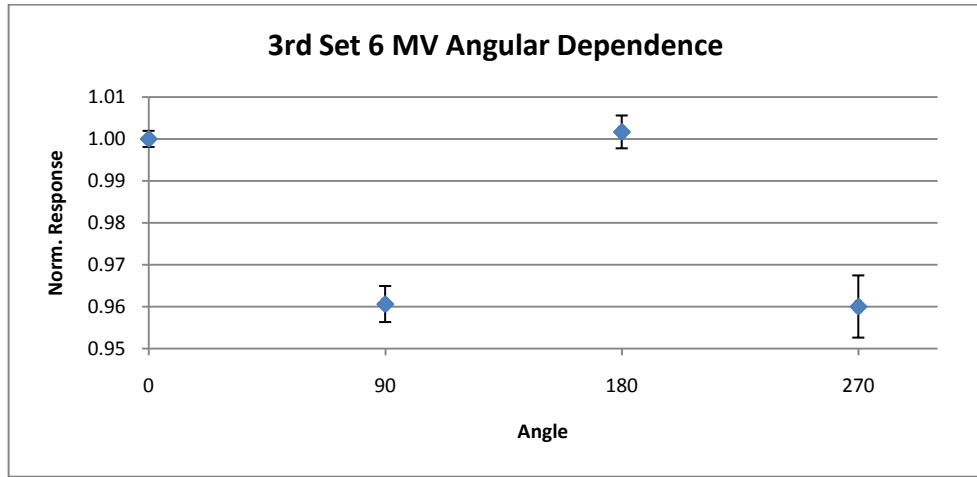
Figure 3.9 Third 6 MV angular dependence data set.
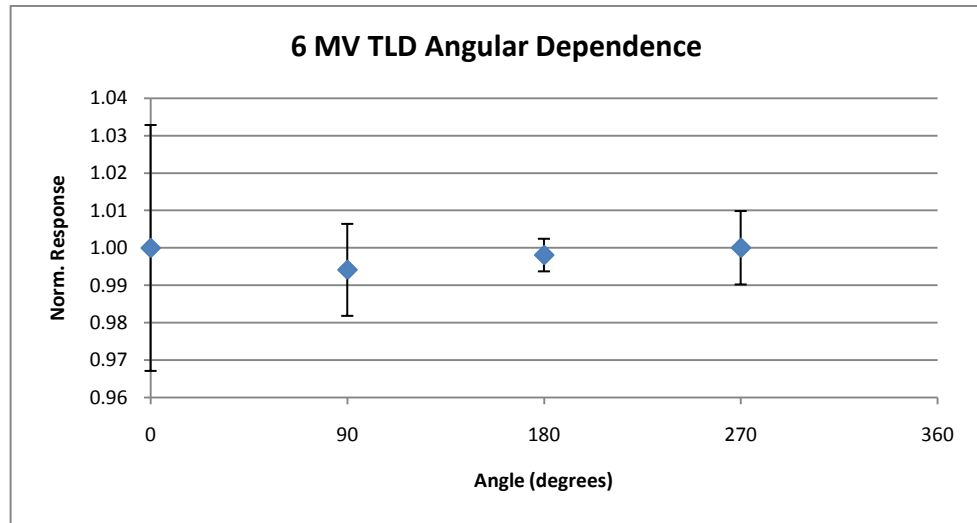
Figure 3.10 6 MV TLD angular dependence data set.
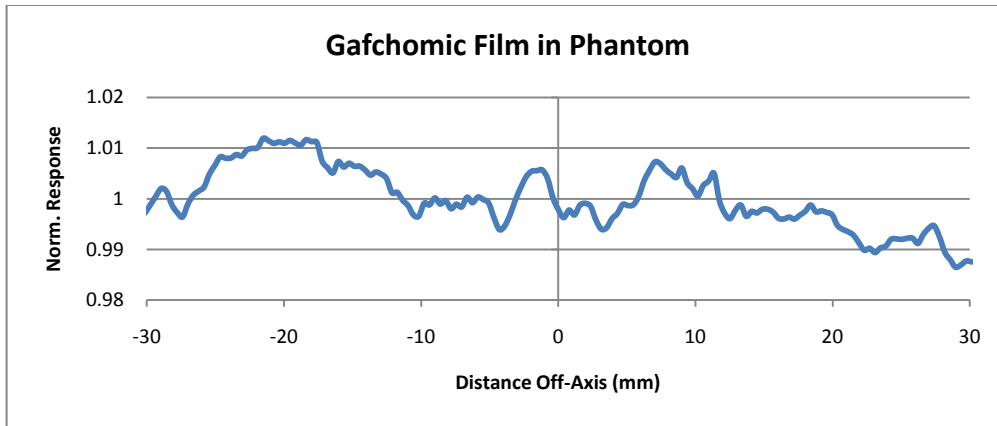
Figure 3.11 Gafchromic film results within the pelvic phantom.
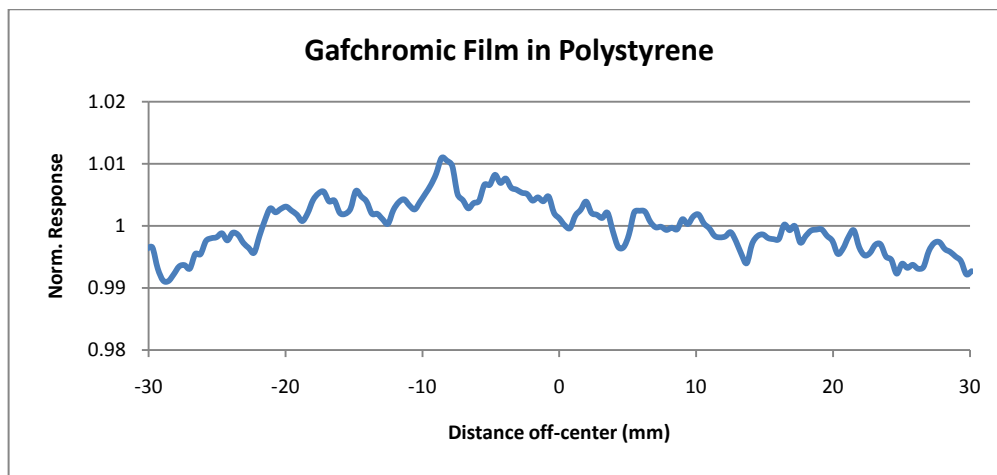
Figure 3.12 Gafchromic film results placed under 10 cm of polystyrene.

The results of the third OSLD irradiation are in agreement with the findings of the first two in that the nanoDots exhibit an angular dependence. Besides the experiment with TLDs, Gafchromic film was irradiated inside the phantom to determine the off-axis dose variation. While the reported off-axis factor was less than 0.5% at 1 cm, a control film was irradiated under 10 cm of polystyrene, which was approximately the same attenuation realized within the phantom. Both films were irradiated to 5 Gy. The results are shown in Figure 3.11 and Figure 3.12, where little off-axis variation seems to be the case. Even at maximum, the variation from

average only approaches 1%, which is not enough to account for the OSLD angular dependence response. With phantom heterogeneity and off-axis possibilities eliminated, there are still other possibilities as to the apparent angular dependence. Dosimeter case effects and absorbed dose could play a factor in the response.

The results of this work disagree with Jursinic's (2007) data using the previous generation InLight dosimeters which stated no dependence within 0.9% experimental uncertainty, and also disagreed with his nanoDot data taken in response to the findings of this study (Jursinic 2010b). However, the thickness of the dosimeter, thickness of the Al_2O_3:C, the density of plastic casing, and casing thickness were all the same in both cases (Jursinic 2007; 2010a).

A possible solution to the under response observed is a result of the scatter conditions existing within the detector casing. The casing density is 1.03 g/cm^3, but air gaps exist between the casing and Al_2O_3:C disk. Using a case thickness of 2 mm, and assuming a cover thickness of 0.36 mm on each side and an Al_2O_3:C disk of 0.3 mm, there remains a total of approximately 0.85 mm of air on each side between the aluminum oxide and casing. A diagram of this condition is shown in Figure 3.13.
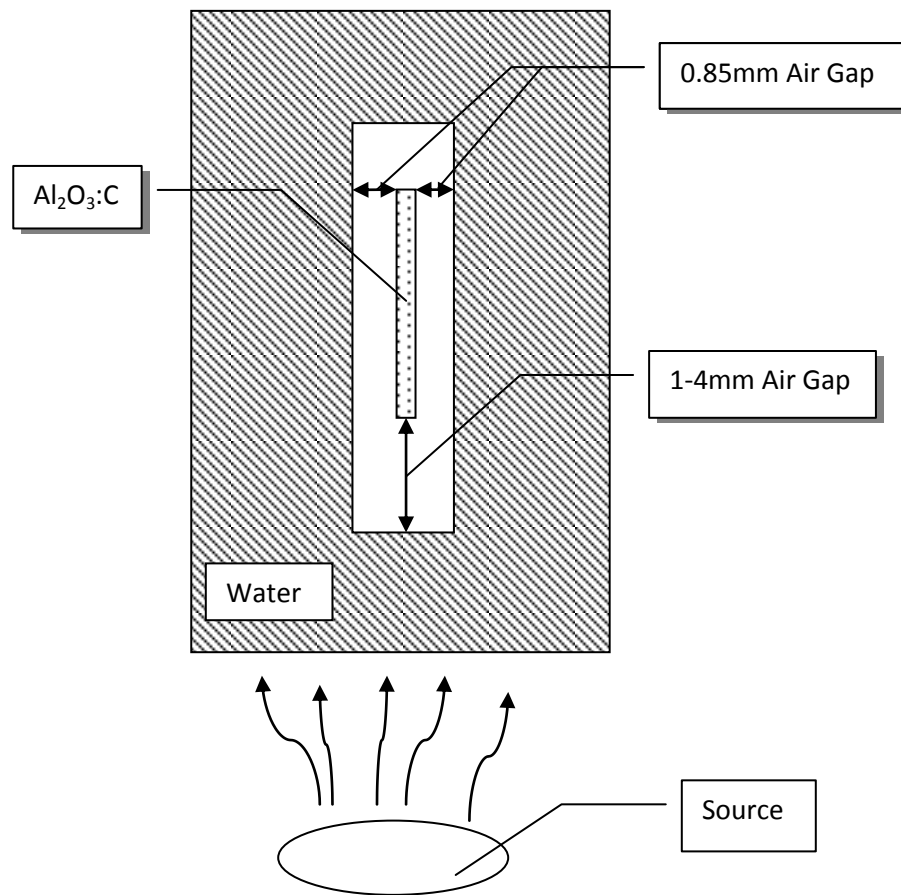
Figure 3.13 Diagram of a nanoDot in water located at an extreme angle relative to the radiation source.

At an extreme angle relative to the incident photons the areal cross-section of the aluminum oxide is very small compared to a perpendicular position (5 mm diameter x 0.3 mm thickness). However, the areal cross-section for scattered photons and electrons from each side becomes higher with increasing scatter angle. Using Klein-Nishina equations, a polar plot is shown in Figure 3.14 displaying the scattered photon energy as a function of angle, recoil electron energy in a Compton process as a function of its recoil angle, as well as a relative cross-section of Compton probability as a function of angle. The calculations are based on a 2 MeV photon, as the effective energy of a 6 MV beam is approximately 2 MeV. While most interactions will be small-angle scattered photons, as the angle from incidence increases, the scattered photon

73

energy decreases and electron energy increases. Since the areal cross-section of the dosimeter increases with angle from incidence for Compton processes, it is plausible the difference in photon and electron spectrum hitting the dosimeter from the sides causes a difference in dose deposition, i.e. partial or uneven volume irradiation. As well, charged particle equilibrium may not be a valid assumption for conditions within the nanoDot.
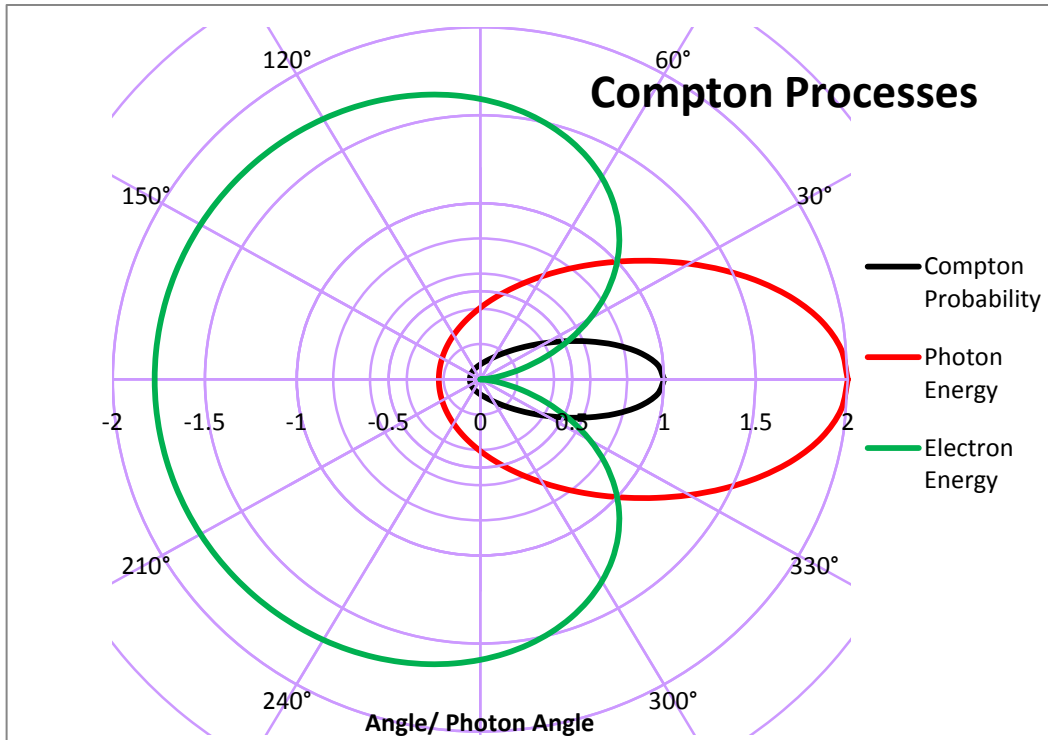
Figure 3.14 Polar graph of Compton interaction probability, recoil electron energy, and scattered photon energy.

The determination of angular dependence is especially important for in vivo dosimetry and multifield treatment and patient quality assurance. For in vivo dosimetry, dosimeters are applied to the patient to ensure correct dose delivery. In such cases, the dosimeter may be at an angle to the incoming radiation beam. As well, for cases such as head & neck, multifield treatments are essential. For the RPC, while this determination does not affect remote dosimetry,

it is very important for anthropomorphic phantom dosimetry like the prostate which has numerous fields.

3.2.1.2 Proton Irradiation

Angular dependence data for protons were measured in two sessions due to time constraints. These sessions were done after the analysis of the photon results and thus the intermediate angles around 90 and 270 were included initially. The first irradiation data set was from angles 0 to 135, and the second set from 180 to 315 with an additional irradiation on the second set at 0 degrees for normalization. The data sets were aggregated and are shown in Figure 3.15. The data shows no angular dependence within statistical uncertainty.
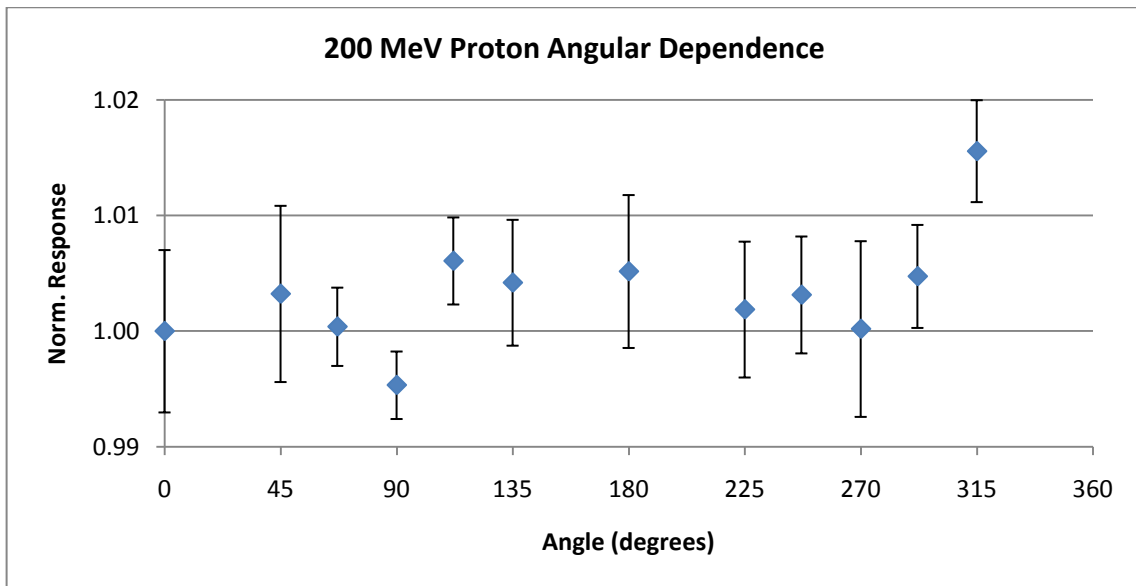
Figure 3.15 200 MeV proton cumulative angular dependence.

As with photons, an additional set of data was measured for protons to ensure reproducibility with previous results. The response was studied at the prime angles, with 3 irradiations of 2 OSLDs at each angle. The results are shown in Figure 3.16.
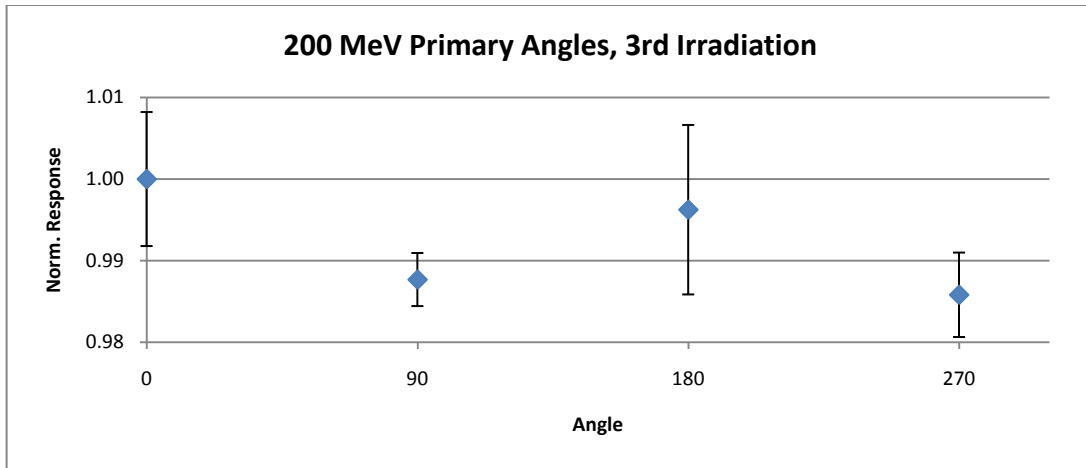
Figure 3.16 Third 200 MeV proton irradiation data set.

The results from this additional irradiation seemed to show a slight angular dependence, differing from the earlier results. A Student's t-test of the averages at 0 and 180 was compared to the results at 90 and 270 to show no statistically significant angular dependence. A fourth experiment was performed to determine if the third irradiation was an anomaly, or whether OSLDs actually do show an angular dependence when irradiated with protons. The setup conditions were the same; results are shown in Figure 3.17. Because of the symmetry observed throughout the study for opposite angles (0 & 180, 90 & 270, etc), only four angles were studied: 0, 45, 90, & 135 degrees.

200 MeV Angular Dependence, 4th Irradiation
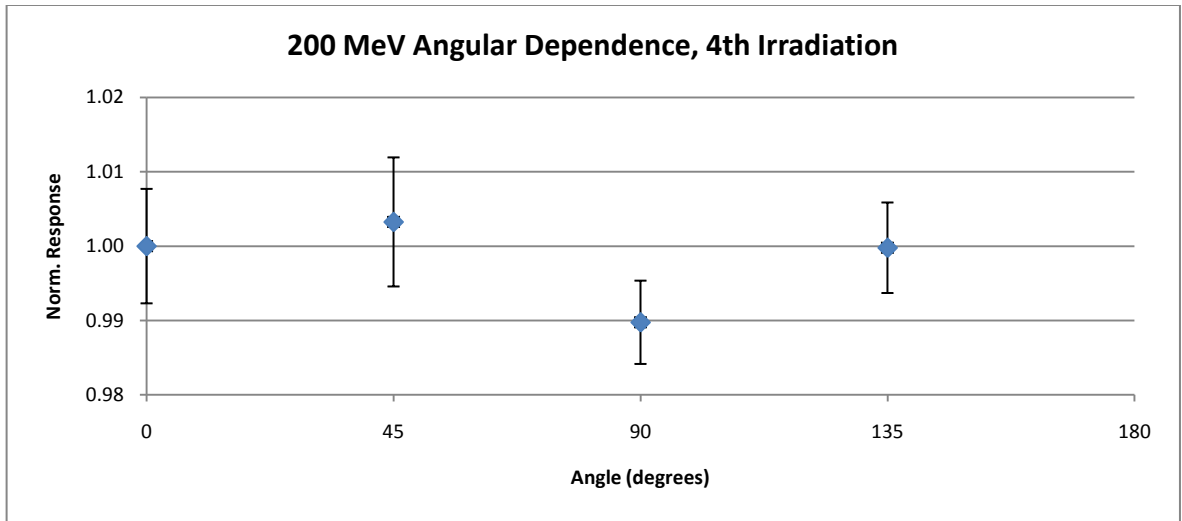
Figure 3.17 Fourth 200 MeV proton irradiation data set.

There again seemed to be a slight under response of approximately 1% at the 90 degree angle, similar to the third irradiation, but not enough for statistical significance. Despite this lack of statistical significance, there were factors unaccounted for in this study that could contribute to angular dependence of Al_2O_3:C in proton irradiations. While this study did not aim to predict the response of Al_2O_3:C within proton beams, previous work and general physics can indicate whether other factors may have affected the dose response of Al_2O_3:C when the dosimeter was irradiated at an angle.

When the dosimeter is placed parallel with the central axis of the radiation field (90 & 270 degrees) the length of the material along the beam path is much longer than when perpendicular. More protons can stop along this longer path length within the material, which will affect response. Since often the majority of dose at a given point within the SOBP is from low-energy protons these protons have a range within the detector's length, causing even more saturation of the detector and fluence perturbation. Because then the number of protons stopping with the detector is increased, the luminescence of a detector parallel to the radiation field should

then be some degree lower than that of a perpendicular dosimeter. However, the absorbed dose of the dosimeter will also increase slightly which would raise the total luminescence.

As well, when the dosimeter is parallel to the proton field the total fluence through the dosimeter is smaller since the incident area has shrunken considerably. This would cause a larger uncertainty, and coupled with the LET effects described above, the true response of the dosimeters is hard to determine. Thus, more experiments must be performed to determine angular dependence, LET within the dosimeter, and the response of such effects with attention to detail of experimental conditions.

3.2.2   Small Cylinder Angular Dependence Irradiation

Data using the small cylinder from Dr. Jursinic were taken in light of the results of the pelvic phantom angular dependence results. Dosimeters at the primary angles (0, 90, 180, & 270) were irradiated, as well as angles ±15 degrees from the extreme angles (75 & 105, 255 & 285). This was done out of convenience as there were already 15 degree marks along the Styrofoam stand to align with, allowing for consistent positioning. The dosimeters were irradiated to 100 MU which resulted in slightly under 100 cGy as the dosimeters were at 1.8 cm, just beyond the d_{max} range of the 6 MV photon beam. The results, shown in Figure 3.18, showed no angular dependence within $\pm1\%$ of the overall average response, although the 0 degree data point is higher than the other average responses.
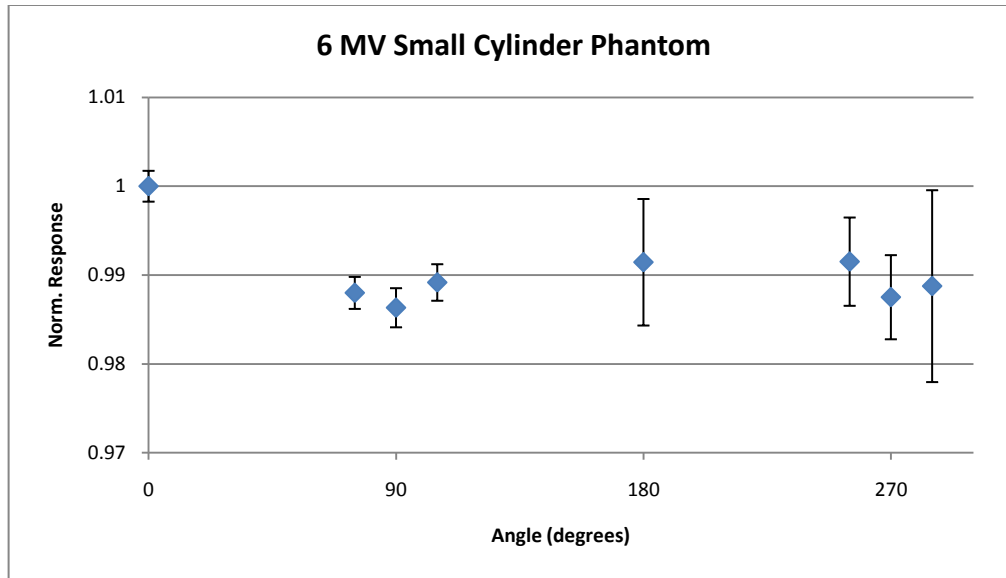
Figure 3.18 6 MV small cylinder angular dependence data set.

3.2.3   Pelvic Insert Angular Dependence Irradiation

Experiments using just the pelvic phantom polystyrene insert were also performed after observing the differing results using the entire pelvic phantom and the small cylinder phantom. The data taken using the pelvic phantom's polystyrene dosimetric insert was done in two sessions. In the first session OSLDs were exposed to a 6 MV photon beam. The major angles (0, 90, 180, & 270) had four OSLDs at each point while the intermediate angles had only two. The results, shown in Figure 3.19, are consistent with the previous results obtained using the entire pelvic phantom, demonstrating an under response of approximately 4% near the extreme angles.
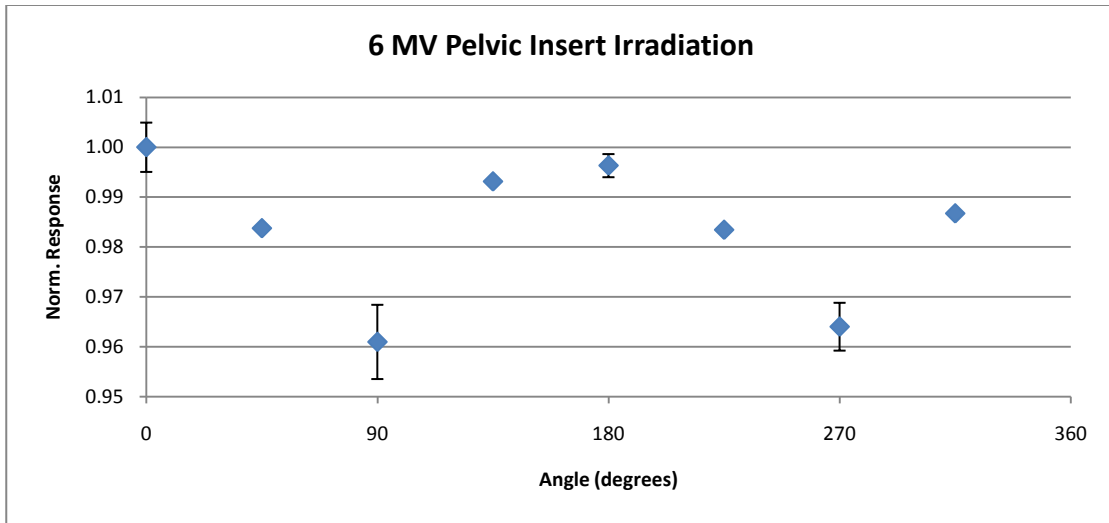
Figure 3.19 6 MV pelvic insert angular dependence data set. Standard deviation error bars were not calculated for the intermediate angles as they were based on only two data values.

The second irradiation session using the phantom insert irradiated OSLDs in an 18 MV photon beam, using the same setup as the 6 MV, with results shown in Figure 3.20. As also for the fourth proton angular dependence irradiation, the symmetry observed throughout the study justified only using four angles: 0, 45, 90, & 135 degrees. The 18 MV angular dependence showed an under response of approximately 3%, as compared to the 4% observed with 6 MV photons. If the results are accurate, it could indicate angular energy dependence. However, more studies should be performed to solidify the results, with careful consideration of the setup and uncontrolled variables to isolate the angular dependence.
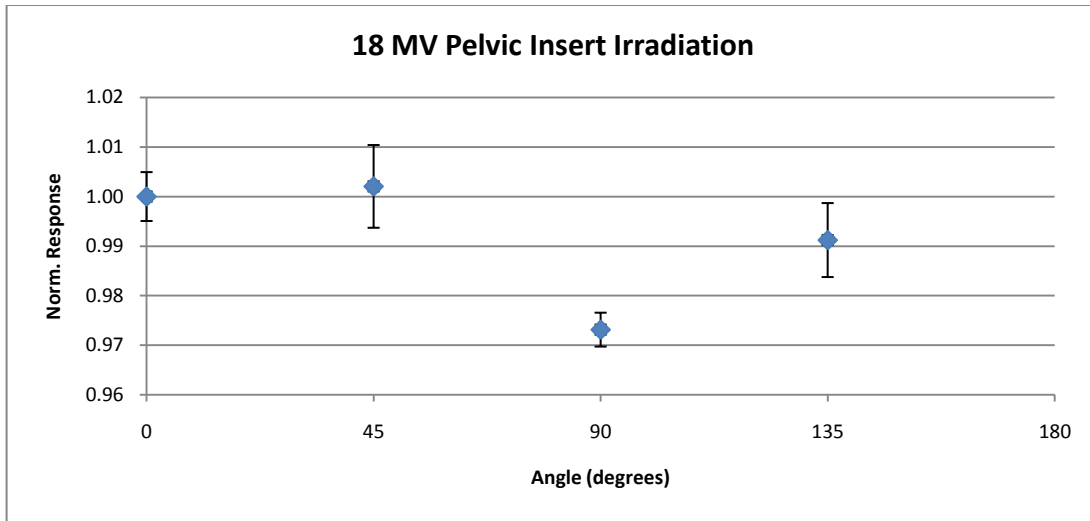
Figure 3.20 18 MV pelvic insert angular dependence data set.

3.3 Fading

The fading characteristic of Al_2O_3:C irradiated in protons may have different results from photons due to the dose distribution and higher percentage contribution from the UV luminescence. Fading data was taken at the PTCH at various points in time. The dosimeters were read in one sitting to minimize uncertainty in reader stability. Yukihara & McKeever (2006a) showed using beta irradiations that the UV contribution to overall signal increases with time post-irradiation as well as with dose. There is an evident drop in signal with time post-irradiation, however, the data are not smooth and could indicate other contributing factors. In the previously mentioned work, the UV signal contribution increased exponentially until reaching an apparent saturation after 200-300 hours. As well, the amount of UV signal contribution depends on total deposited dose, but constitutes approximately 30% of the signal up to 10 Gy with the filters used in that study. Since the RPC does not allow the OSL dosimeters to receive more than 10 Gy accumulated dose, a dose-dependent proton fading factor should not be needed.

The results of OSLD proton fading measurements are shown in Figure 3.21, and are compared with other fading results. Data from Yukihara *et al.* (2010) show the overall fading response of Luxel dosimeters irradiated with beta particles in both the short-term and long-term using the microStar reader. In the long term study, the response showed a signal fading of roughly 3% after 30 days compared to one day post-irradiation. Those results are similar to the results obtained in this study for protons considering the experimental uncertainty. As well, the RPC has investigated the fading of the nanoDot in photons and is consistent with the results obtained here with protons.
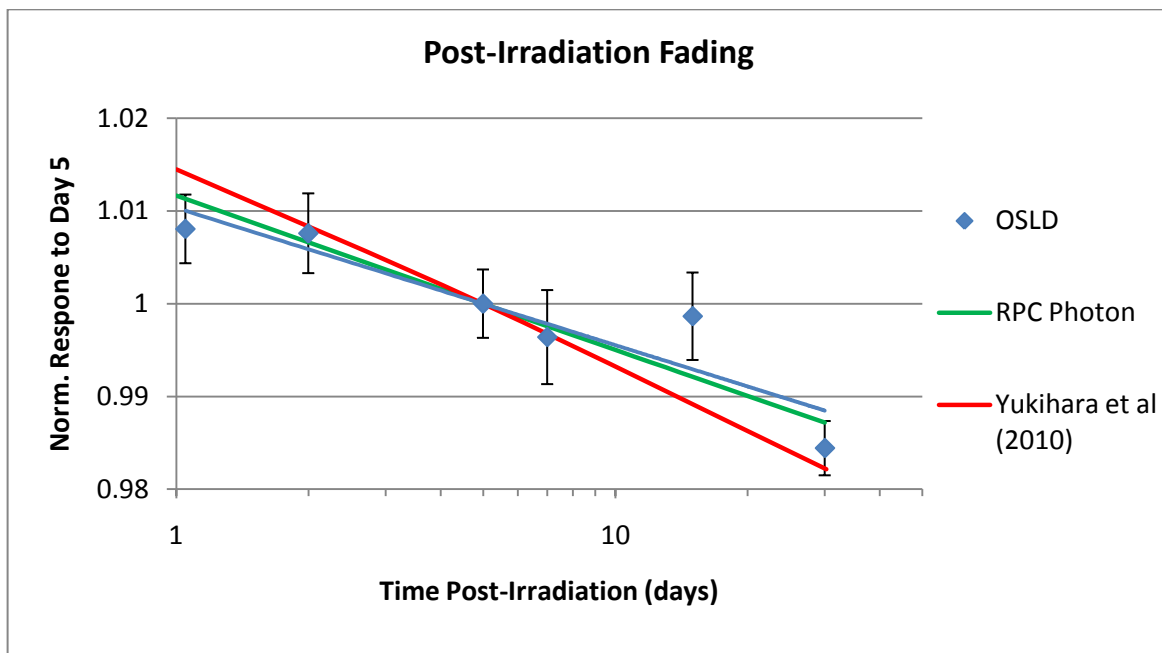
Figure 3.21 OSLD proton fading results compared to the RPC fading data in photons and the results of Yukihara *et al.* (2010).

Since the results show a similar signal fading to that of low-LET irradiations it is possible to preliminarily apply the same fading correction for photons to protons. Again, since the accumulated dose in RPC OSLDs is less than 10 Gy, the dose dependence should not affect the results. The fading response found in this study are similar to the consensus of other work

(Homnick 2008; Gasparian 2006; Jursinic 2007; Viamonte *et al.* 2008), showing a drop of 2-3% over the first several days post-irradiation.

It should be noted that because of the small energy dependence, shown in the next section, the conclusions of the fading study can safely be applied to therapeutic proton energies.

3.4 Proton Energy Dependence

LET changes with proton energy, and it was desired to know the response of OSLDs across a range of therapeutic energies. Although LET dependence has been studied somewhat in literature elsewhere, each dosimetry system can respond differently for the same dosimeter or parameters because of different reader optical filters, thus necessitating a study of energy dependence for the RPC's dosimetry protocol. Data for this observation was taken from the 200 MeV OSL/TL comparison, the 160 MeV fading data, and a separate 250 MeV irradiation. These energies represent the clinical range of protons used at the PTCH. For the 160 MeV data, the set read 5 days post-irradiation was used as it was the same waiting time of the other OSLDs in the other experiments. The results comparing the different energies are shown in Figure 3.22.

In the context of this study the term energy dependence study is a misnomer. Because of the physical set up, the results are not showing energy dependence explicitly. The dosimeters were always in the middle of the SOBP, meaning that at any given point along it there is a spectrum of proton energies, and thus LETs. An LET vs. range tool (Zajic 2001) was used to approximate an average LET at the dosimeter location based on residual energy. The nominal proton energy, average LET, SOBP, absorbed dose at the nominal energy, and determined energy dependence correction factor are shown in

83

Table 3.1 and Figure 3.22. The reported dose values are the apparent dose in cGy after being exposed to 100 MU (100 cGy to water at the center of the SOBP).

Proton Energy (MeV;SOBP; average LET)	Delivered dose to water (cGy)	Experimental Absorbed dose (cGy)	Al_2O_3 Absorbed dose at nominal energy (cGy) (Equation 1.12)	Experimental K_e
160; 6; 2.1	100.0	90.75±0.33	91.9	1.102
200; 10; 1.5	100.0	93.78±0.18	92.1	1.066
250; 10; 1.5	100.0	91.56±0.37	92.3	1.092

Table 3.1 Proton OSL determined dose for this study and the absorbed dose at the nominal energy, all assuming a 100 cGy irradiation. The SOBP value is in cm while the LET value is an estimation of LET at the dosimeter location in keV/μm. The experimental energy correction factor, K_e, for each energy is listed as well.
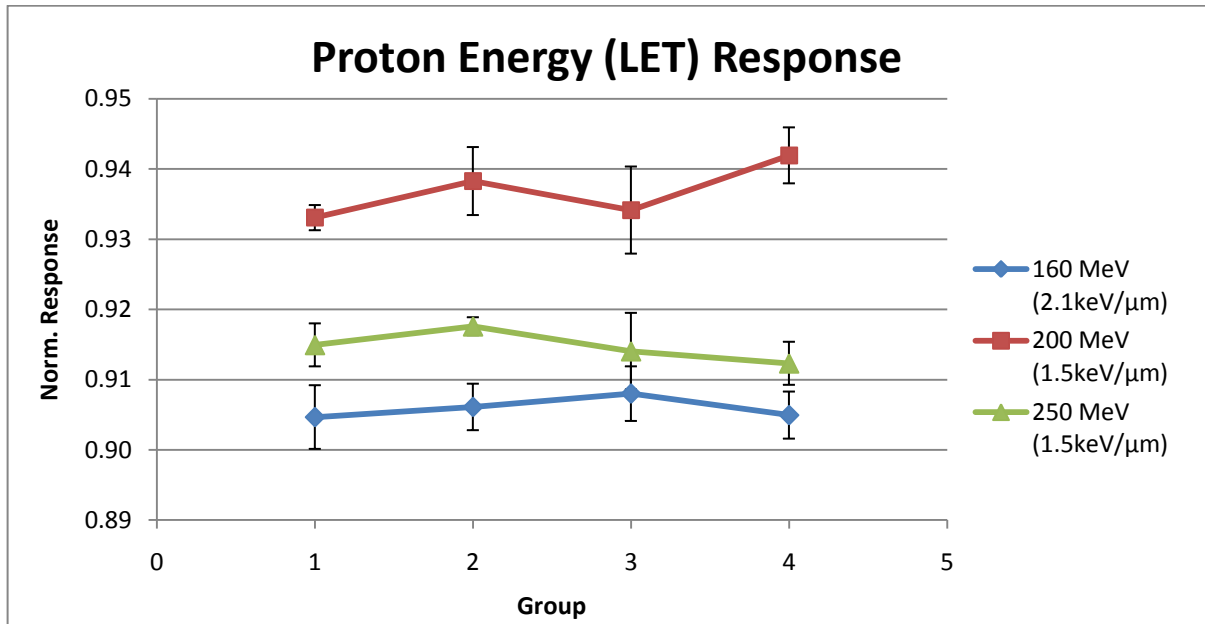
Figure 3.22 Results of proton data taken at three energies. Each experiment is listed with its nominal energy and LET at dosimeter point.

Figure 3.22 shows that for all proton energies tested, the OSLDs consistently under responded to the calculated dose. There are two reasons to expect an under response: absorbed dose, as discussed in Section 1.7.2, and trap saturation due to uneven dose distribution of HCPs.

It is important to distinguish between these two factors. One is due to the material composition and the other to dose deposition. In this OSL/TL experiment the doses and energies were low enough that trap saturation was not observed, which would manifest by showing consistent differences between absorbed dose expectations and measurements. The 200 MeV irradiation had a greater response that the 160 and 250 MeV. The 200 MeV experiment was performed at a different time than the other two, and reader uncertainty and dose delivery constancy are thought to be related to this over response.

Gasparian (2006) studied the efficiency of reader & filter combination in proton beams, including the microStar reader. Efficiency for the same dose and dosimeter ranged from 0.90 to over 1.10 between several reader and filter combinations. Her results of the microStar showed efficiency of approximately 0.90 to 0.96, consistent with the results of this study.

Defining the experiment in terms of LET is more accurate than using the nominal energy, but the effective LET is only estimated, causing uncertainty. Attempts at defining the average LET in HCP beams has been studied in TLDs for space dosimetry (Berger *et al.* 2002; Hajek *et al.* 2002) but has yet to be done in OSLDs, although studies are being done. Since the RPC remotely audits proton beams in reference conditions, correction factors can be attached either to the nominal beam energy and SOBP width or to the effective LET.

3.5 Uncertainty Analysis

An analysis of the uncertainty of the experimental results is imperative for transparent evaluation and derivation of total uncertainty as reported by the RPC. In any experiment there will be some kind of fluctuation in results, causing a level of uncertainty, termed Type A, or statistic uncertainty. Type B uncertainty deals with non-statistical uncertainties such as ionization

chamber calibration and standards calibration. This study calculated uncertainties according to the experimental standard deviation of the data (GUM 2008), described as:

$$s(m) = \sqrt{\frac{\sum_{k=1}^{n}(m_k - \bar{m})^2}{n-1}}$$

Equation 3.8 Standard deviation definition.

where $s(m)$ is the standard deviation, m_k is the kth measurement, and $\bar{m}$ is the arithmetic mean of the data consisting of n samples.

As well, data uncertainties in this study were reported in percentage. This percentage is calculated by using, and is equivalent to, the coefficient of variation, described as:

$$COV = \frac{s}{\bar{m}}$$

Equation 3.9 Coefficient of variation definition.

where s is the standard deviation and $\bar{m}$ is the arithmetic mean, just as in Equation 3.8.

Kirby *et al.* (1992) describes the statistical uncertainty analysis of TLDs used in conjunction with the RPC's mailable dosimetry program which states the uncertainties of each correction factor and TL readings. Since a full determination of the correction factors for OSLDs has yet to be completed, nor historic data like the RPC has for TLDs, a full comparison of uncertainties cannot be done. Even so, for TLDs the measurement of uncertainty according to the RPC calculations for three samples, i.e. the standard error, is 1.3% for samples irradiated to the same dose which corresponds to 5.0% uncertainty at the 93% confidence level. The two largest contributors of uncertainty in dose calculation according to Kirby et al were the TLD readings followed by the energy correction factor. However, each batch of TLD powder can have different

86

characteristics and thus an individual batch may have slightly smaller or larger correction factor uncertainties. For OSLDs, as the correction factors are determined the uncertainty value can be updated. Since the sample readings introduce the most uncertainty in the TLD calculations, it could be assumed that it is the same case for OSLDs.

Chapter 4 - Conclusion

4.1 Conclusion

In this study, the response of optically stimulated luminescence detectors, specifically nanoDots made of Al_2O_3:C from Landauer, was investigated and compared to that of thermoluminescent detectors for selected energies and situations. As well, the response of the OSLDs at various angles relative to the incident radiation beam for both photons and protons was investigated.

Both OSLDs and TLDs were placed within a custom phantom to compare the response in 6 MV photons and various therapeutic proton energies in full scatter conditions to mimic an anthropomorphic phantom. The response of OSLDs and TLDs was desired to be within 3% of each other, and was so for 6 MV photons and cobalt-60. OSLD response in therapeutic energy proton beams is reduced due to a difference in absorbed dose and saturation of the local charge traps, causing a significant under response compared to TLDs. If the Al_2O_3:C OSLDs are corrected for absorbed dose in proton beams, the accuracy would be within 3% of TLDs and the calculated dose.

When irradiated at various angles in 6 MV photons inside the RPC pelvic phantom, the OSLDs were shown to have a response dependence of -4% at the extreme angles (90 & 270). However, experiments using a simple cylindrical phantom showed no angular dependence within $\pm$1%. When irradiated in protons, the OSLDs did not show angular dependence within $\pm$1.5%.

A study of signal fading of OSLDs irradiated in protons was done for various times post-irradiation ranging from 1 month to 1 day and compared to other results in photons. The results showed a drop in signal of 2-3% at 30 days post-irradiation compared to the response on day 1, consistent with the RPC's fading data of OSLDs in photons.

88

The hypothesis of this study was: *OSLDs can be used to measure dose in both photon and proton beams with accuracy that is within 3% of TLD response and can be characterized in full-phantom conditions.*

Based on the results of this study, the accuracy of OSLDs are within 3% of TLD response at 6 MV and can be accurate to within 3% if an Al_2O_3 absorbed dose correction is applied for protons. The OSLD photon fading correction factor currently in place at the RPC is sufficient for fading correction of OSLDs irradiated to 100 cGy in proton beams. If Al_2O_3:C nanoDots are used for multifield treatment QA tests some kind of angular dependence correction factor must be in place, or at least an awareness of the possible under response of the dosimeter.

4.2 Future Work

Future work in OSLDs at the RPC could include a more comprehensive study of OSLD fading in protons to achieve better statistics and then compared to the results of low-LET irradiations. As well, fading for a range of doses could be performed to determine if signal fading in protons is dose dependent.

Although general absorbed dose Monte Carlo calculations have been done, one way to determine whether angular dependence is inherent to the crystal or caused by an external factor would be to perform a simulation using Monte Carlo, being careful to reconstruct and analyze the air gap between the casing and dosimeter.

A fuller and more precise characterization of OSLDs in proton beams would be beneficial to the RPC, including responses at more energies and combinations of SOBPs as well as dose linearity response. This would also contribute to the possibility of using OSLDs for proton therapy treatment QA.

89

References

Akselrod, M. S. & V. S. Kortov (1990). "Thermoluminescent and Exoemission properties of New High-Sensitivity TLD anion-Al_2O_3:C Crystals." <u>Radiation Protection Dosimetry</u> **33**: 123-126.

Akselrod, M. S., V. S. Kortov & E. A. Gorelova (1993). "Preparation and Properties of Al_2O_3:C." <u>Radiation Protection Dosimetry</u> **47**: 159-164.

Akselrod, M. S. & S. W. S. McKeever (1999). "A radiation dosimetry method using pulsed optically stimulated luminescence." <u>Radiation Protection Dosimetry</u> **81**(3): 167-176.

Akselrod, M. S., L. Bøtter-Jensen & S. W. S. McKeever (2007). "Optically stimulated luminescence and its use in medical dosimetry." <u>Radiation Measurements</u> **41**: S78-S99.

Almond, P. R., P. J. Biggs, B. M. Coursey, W. F. Hanson, M. S. Huq, R. Nath & D. W. Rogers (1999). "AAPM's TG-51 protocol for clinical reference dosimetry of high-energy photon and electron beams." <u>Med Phys</u> **26**(9): 1847-1870.

Andersen, C. E., C. J. Marckmann, M. C. Aznar, L. Bøtter-Jensen, F. Kjaer-Kristoffersen & J. Medin (2006). "An algorithm for real-time dosimetry in intensity-modulated radiation therapy using the radioluminescence signal from Al_2O_3:C." <u>Radiation Protection Dosimetry</u> **120**: 7-13.

Andreo, P., D. T. Burns, K. Hohlfeld, M. S. Huq, T. Kanai, F. Laitano, V. Smyth & S. Vynckier (2000). "Absorbed dose determination in external beam radiotherapy: An international code of

practice for dosimetry based on standards of absorbed dose to water." <u>IAEA Technical Report Series No. 398</u>.

Antonov-Romanovskii, V. V., I. F. Keirum-Marcus, M. S. Poroshina & Z. A. Trapeznikova (1956). IR stimulable phosphors. <u>In: Conference of the Academy of Sciences of the USSR on the Peaceful Uses of Atomic Energy</u>. Moscow, USAEC Report AEC-tr-2435**:** 239-250.

Aznar, M. C., C. E. Andersen, L. Bøtter-Jensen, S. A. Bäck, S. Mattsson, F. Kjar-Kristoffersen & J. Medin (2004). "Real-time optical-fibre luminescence dosimetry for radiotherapy: physical charactersitcs and applications in photon beams." <u>Physics in Medicine and Biology</u> **49**: 1655-1669.

Berger, M. J., J. S. Coursey, M. A. Zucker & J. Chang (2005). "Stopping-Power and Range Tables for Electrons, Protons, and Helium Ions." from http://www.nist.gov/physlab/data/star/index.cfm.

Berger, T., M. Hajek, W. Schoner, M. Fugger, N. Vana, Y. Akatov, V. Shurshakov, V. V. Arkhangelsky & D. Kartashov (2002). "Application of the high-temperature ratio method for evaluation of the depth distribution of dose equivalent in a water-filled phantom on board space station MIR." <u>Radiation Protection Dosimetry</u> **100**: 503-506.

Bos, A. J. J. (2001). "High sensitivity thermolumienscence dosimetry." <u>Nucl Instrum Methods Phys Res B</u> **184**: 3-28.

Bøtter-Jensen, L., N. A. Larsen, B. G. Markey & S. W. S. McKeever (1997). "Al$_2$O$_3$:C as a sensitive OSL dosemeterfor rapid assessment of enviornmental photon dose rates." Radiation Measurements **27**: 295-298.

Bøtter-Jensen, L., S. W. S. McKeever & A. G. Wintle (2003). Optically Stimulated Luminescence Dosimetry, Elsevier.

Bulur, E. & H. Y. Göksu (1998). "OSL from BeO ceramics: new observations from an old material." Radiation Measurements **29**: 639-650.

Chen, S. W., X. T. Wang, L. X. Chen, Q. Tang & X. W. Liu (2009). "Monte Carlo evaluations of the absorbed dose and quality dependence of Al$_2$O$_3$ in radiotherapy photon beams." Med Phys **36**: 4421-4424.

Edmund, J. M., C. E. Andersen & S. Greilich (2007). "A track structure model of optically stimulated luminescence from Al$_2$O$_3$:C irradiated with 10-60 MeV protons." Nucl Instrum Methods Phys Res B **262**: 261-275.

Followill, D. S., D. R. Evans, C. Cherry, A. Molineu, G. Fisher, W. F. Hanson & G. S. Ibbott (2007). "Design, development, and implementation of the Radiological Physics Center's pelvis and thorax anthropomorphic quality assurance phantoms." Med Phys **34**: 2070-2076.

Gasparian, P. B. (2006). Methodological Developments for Application of Optically Stimulated Luminescence (OSL) in Medical Dosimetry. Stillwater, OK, Oklahoma State University. **Masters Thesis**.

Gaza, R., E. G. Yukihara & S. W. McKeever (2004). "The response of thermally and optically stimulated luminescence from Al2O3:C to high-energy heavy charged particles." <u>Radiat Meas</u> **38**(4-6): 417-420.

Gaza, R., E. G. Yukihara & S. W. McKeever (2006). "The use of optically stimulated luminescence from AL2O3:C in the dosimetry of high-energy heavy charged particle fields." <u>Radiat Prot Dosimetry</u> **120**(1-4): 354-357.

Grimmeiss, H. G. & L. Ledebo (1975). "Photo-ionization of deep impurity levels in semiconductors with non-parabolic bands." <u>J Phys C: Solid State Phys</u> **8**: 2615-2626.

GUM (2008). Internation Organization for Standardization Guide to the Expression of Uncertainty in Measurement (GUM). <u>ISO/IEC Guide 98-3:2008</u>. Geneva, Switzerland.

Hajek, M., T. Berger, W. Schoner, L. Summerer & N. Vana (2002). "Dose assessment of aircrew using passive detectors." <u>Radiation Protection Dosimetry</u> **100**: 511-514.

Homnick, J. M. (2008). Evaluation of Aluminum-Oxide (Al_2O_3:C) Optically Stimulated Luminescence (OSL) Dosimeters as a Potential Alternative to Thermoluminescent Dosimeters

(TLDs) for Remote Dosimetry Services. Houston, TX, The University of Texas Health Science Center at Houston Graduate School of Biomedical Sciences. **Masters Thesis**.

Hubbell, J. H. & S. M. Seltzer (2004). "Tables of X-Ray Mass Attenuation Coefficients and Mass Energy-Absorption Coefficients." from http://www.nist.gov/physlab/data/xraycoef/index.cfm.

Huntley, D. J., D. I. Godfrey-Smith & M. L. W. Thewalt (1985). "Optical dating of sediments." Nature **313**(10): 105-107.

Ibbott, G. S., D. S. Followill & J. F. Aguirre (2008). Remote audit of proton beams with TLD. PTCOG 47. University of Florida Proton Therapy Institute, Jacksonville, FL.

ICRU (1993). Stopping Power and Ranges for Protons and Alpha Particles. ICRU Report 49. Bethesda, MD.

Jursinic, P. A. (2007). "Characterization of optically stimulated luminescent dosimeters, OSLDs, for clinical dosimetric measurements." Med Phys **34**(12): 4594-4604.

Jursinic, P. A. (2010). "Changes in optically stimulated luminescent dosimeter (OSLD) dosimetric characteristics with accumulated dose." Med Phys **37**(1): 132-140.

Jursinic, P. A. (2010). Personal email. J. R. Kerns.

Kirby, T. H., W. F. Hanson, R. J. Gastorf, C. H. Chu & R. J. Shalek (1986). "Mailable TLD system for photon and electron therapy beams." Int J Radiat Oncol Biol Phys **12**(2): 261-265.

Kirby, T. H., W. F. Hanson & D. A. Johnston (1992). "Uncertainty analysis of absorbed dose calculations from thermoluminescence dosimeters." Med Phys **19**(6): 1427-1433.

Lucovsky, G. (1964). "On the photonionisation of deep impurity centers in semiconductors." Sol State Commun **3**: 299-302.

Mancosu, P., D. Ripamonti, I. Veronese, M. C. Cantone, A. Giussani & G. Tosi (2005). "Angular dependence of the TL reading of thin α-Al$_2$O$_3$:C dosemeters exposed to different beta spectra." Radiation Protection Dosimetry.

Markey, B. G., L. E. Colyott & S. W. S. McKeever (1995). "Time-resolved optically stimulated luminescence from α-Al$_2$O$_3$:C." Radiation Measurements **24**: 457-463.

McKeever, S. W. S., M. S. Akselrod, L. E. Colyott, L. N. Agersnap, J. C. Polf & V. H. Whitley (1999). "Characterisation of Al$_2$O$_3$ for use in thermally and optically stimulated luminescence dosimetry." Radiation Protection Dosimetry **84**: 163-168.

Miller, S. D. & M. K. Murphy (2006). "Technical performance of the Luxel Al_2O_3:C optically stimulated luminsecence dosemeter element at radiation oncology and nuclear accident dose levels." Radiation Protection Dosimetry.

Mobit, P., E. Agyingi & G. Sandison (2006). "Comparison of the energy-response factor of LiF and Al_2O_3 in radiotherapy beams." Radiat Prot Dosimetry **119**(1-4): 497-499.

Orton, C. G. & J. B. Seibert (1972). "The measurement of teletherapy unit timer errors." Phys Med Biol **17**(2): 198-205.

Perks, C. A., G. Le Roy & B. Prugnaud (2007). "Introduction of the InLight monitoring service." Radiation Protection Dosimetry.

Perks, C. A., C. Yahnke & M. Million (2008). Medical dosimetry using Optically Stimulated Luminescence dots and microStar readers. 12th International Congress of the International Radiation Protection Association. Buenos Aires, Argentina.

Polf, J. C., E. G. Yukihara, M. S. Akselrod & S. W. S. McKeever (2004). "Real-time luminescence from Al_2O_3 fiber dosimeters." Radiation Measurements **38**: 227-240.

Reft, C. S. (2009). "The energy dependence and dose response of a commercial optically stimulated luminescent detector for kilovoltage photon, megavoltage photon, and electron, proton, and carbon beams." Med Phys **36**(5): 1690-1699.

Sahoo, N., X. R. Zhu, B. Arjomandy, G. Ciangaru, M. Lii, R. Amos, R. Wu & M. Gillin (2008). "A procedure for calculation of monitor units for passively scattered proton radiotherapy beams." Med Phys **35**(11): 5088-5097.

Sawakuchi, G., E. Yukihara, S. W. S. McKeever & E. Benton (2008). "Overlap of heavy charged particle tracks and the change in shape of optically stumulated luminescence curves of Al_2O_3:C dosimeters." Radiation Measurements **43**: 194-198.

Sawakuchi, G. O., E. Yukihara, S. W. S. McKeever, E. Benton, R. Gaza, Y. Uchihori, N. Yasuda & H. Kitamura (2008). "Relative optically stimulated luminsecence and thermoluminscence efficiences of Al_2O_3:C dosimeters to heavy charged particles with energies relavent to space and radiotherapy dosimetry " Journal of Applied Physics **104**: 124903-124901-124910.

Schembri, V. & B. J. Heijmen (2007). "Optically stimulated luminescence (OSL) of carbon-doped aluminum oxide (Al_2O_3:C) for film dosimetry in radiotherapy." Med Phys **34**: 2113-2118.

Task Group 21, Radiation Therapy Committee, American Association of Physicists in Medicine (1983). "A protocol for the determination of absorbed dose from high energy photon and electron beams." Med Phys **10**: 741-772.

Viamonte, A., L. A. da Rosa, L. A. Buckley, A. Cherpak & J. E. Cygler (2008). "Radiotherapy dosimetry using a commercial OSL system." Med Phys **35**(4): 1261-1266.

Whitley, V. H. & S. W. S. McKeever (2000). "Photoionization of deep centers in Al_2O_3." Journal of Applied Physics **87**: 249-256.

Yoshimura, E. M. & E. G. Yukihara (2006). "Optically stimulated luminescence of magnesium aluminate ($MgAl_2O_4$) spinel." Radiation Measurements **41**: 163-169.

Yukihara, E. G., V. H. Whitley, J. C. Polf, D. M. Klein, S. W. S. McKeever, A. E. Akselrod & M. S. Akselrod (2003). "The effects of deep trap population on the thermoluminescence of Al_2O_3:C." Radiation Measurements **37**: 627-638.

Yukihara, E. G., R. Gaza, S. W. McKeever & C. G. Soares (2004). "Optically stimulated luminescence and thermoluminescence efficiencies for high-energy heavy charged particle irradiation in Al2O3:C." Radiat Meas **38**(1): 59-70.

Yukihara, E. G., V. H. Whitley, S. W. McKeever, A. E. Akselrod & M. S. Akselrod (2004). "Effect of high-dose irradiation on the optically stimulated luminescence of Al2O3:C." Radiat Meas **38**(3): 317-330.

Yukihara, E. G., E. M. Yoshimura, T. D. Lindstrom, S. Ahmad, K. K. Taylor & G. Mardirossian (2005). "High-precision dosimetry for radiotherapy using the optically stimulated luminescence technique and thin Al2O3:C dosimeters." Phys Med Biol **50**(23): 5619-5628.

Yukihara, E. G. & S. W. S. McKeever (2006). "Spectroscopy and optically stimulated lumiescence of Al_2O_3:C using time-resolved measurements." <u>Journal of Applied Physics</u> **100**: 083512-083511-083519.

Yukihara, E. G. & S. W. S. McKeever (2006). "Ionisation density dependence of the optically and thermally stimulated luminescence from Al2O3:C." <u>Radiat Prot Dosimetry</u> **119**(1-4): 206-217.

Yukihara, E. G., G. Sawakuchi, S. Guduru, S. W. S. McKeever, R. Gaza, E. Benton, H. Yasuda, Y. Uchihori & H. Kitamura (2006). "Application of the optically stimulated luminescence (OSL) technique in space dosimetry." <u>Radiation Measurements</u> **41**: 1126-1135.

Yukihara, E. G., G. Mardirossian, M. Mirzasadeghi, S. Guduru & S. Ahmad (2008). "Evaluation of Al2O3:C optically stimulated luminescence (OSL) dosimeters for passive dosimetry of high-energy photon and electron beams in radiotherapy." <u>Med Phys</u> **35**(1): 260-269.

Yukihara, E. G. & S. W. S. McKeever (2008). "Optically stimulated luminescence (OSL) dosimetry in medicine." <u>Phys Med Biol</u> **53**(20): R351-379.

Yukihara, E. G., P. B. Gasparian, G. Sawakuchi, C. Ruan, S. Ahmad, C. Kalavagunta, W. J. Clouse, N. Sahoo & U. Titt (2010). "Medical applications of optically stimulated lumiescence dosimeters (OSLDs)." <u>Radiation Measurements</u> **45**: 658-662.

Zajic, V. (2001). "Energy vs. LET vs. Range calculation v1.24."

http://tvdg10.phy.bnl.gov/let.html.

Vita

James Russell Kerns was born in Phoenix, Arizona on October 22, 1986 to Brian and Christine Kerns. After completing high school as valedictorian at Christian Heritage School, he entered into Point Loma Nazarene University, San Diego, California. He graduated cum laude in May of 2008 with a Bachelor of Science degree in Engineering/Physics. In August of 2008, he entered into the Medical Physics program at the University of Texas Health Science Center at Houston Graduate School of Biomedical Sciences.

Permanent Address:

21830 Crystal Ann Ct.

Perris, CA 92570